

Carbon isotope evidence for the global physiology of Proterozoic cyanobacteria

Sarah J. Hurley^{1,2,*}, Boswell A. Wing¹, Claire E. Jasper¹, Nicholas C. Hill^{2,3}, Jeffrey C. Cameron^{2,3,4*}

Ancestral cyanobacteria are assumed to be prominent primary producers after the Great Oxidation Event [≈ 2.4 to 2.0 billion years (Ga) ago], but carbon isotope fractionation by extant marine cyanobacteria (α -cyanobacteria) is inconsistent with isotopic records of carbon fixation by primary producers in the mid-Proterozoic eon (1.8 to 1.0 Ga ago). To resolve this disagreement, we quantified carbon isotope fractionation by a wild-type planktic β -cyanobacterium (*Synechococcus* sp. PCC 7002), an engineered Proterozoic analog lacking a CO_2 -concentrating mechanism, and cyanobacterial mats. At mid-Proterozoic pH and $p\text{CO}_2$ values, carbon isotope fractionation by the wild-type β -cyanobacterium is fully consistent with the Proterozoic carbon isotope record, suggesting that cyanobacteria with CO_2 -concentrating mechanisms were apparently the major primary producers in the pelagic Proterozoic ocean, despite atmospheric CO_2 levels up to 100 times modern. The selectively permeable microcompartments central to cyanobacterial CO_2 -concentrating mechanisms (“carboxysomes”) likely emerged to shield rubisco from O_2 during the Great Oxidation Event.

INTRODUCTION

Members of the phylum Cyanobacteria are the only extant bacteria capable of oxygenic photosynthesis, leading to the inference that ancestral cyanobacteria were responsible for the Paleoproterozoic accumulation of atmospheric O_2 known as the Great Oxidation Event [GOE; 2.4 to 2.0 billion years (Ga) ago] (1). Although estimates of when oxygenic photosynthesis originated span a billion years—from sometime in the Paleoarchean eon (3.6 to 3.2 Ga ago) to immediately preceding the GOE [Fig. 1 and the Supplementary Materials (SM)] [e.g., (2, 3)]—the oxidative impact of this metabolism across the GOE was profound. Atmospheric O_2 concentrations increased by up to 100 million-fold (1, 4) relative to CO_2 concentrations (Fig. 1), while primary productivity rose to potentially modern levels (5). Following the GOE, the trajectories of both atmospheric O_2 concentrations and primary productivity appear to have stalled, with atmospheric oxygen falling to somewhere between 0.1 and 10% of present atmospheric levels [1 PAL = 210,000 parts per million (ppm) O_2 ; Fig. 1] (1, 6) and oxygenic primary production decreasing to less than 10% of modern values (5). Stabilization of the Earth system at this intermediate state of oxygenic primary production characterized much of the Proterozoic eon (7, 8). There are a variety of hypotheses for why this stasis defined the Proterozoic Earth system [e.g., (9–12)] and the physiology of ancestral cyanobacteria features prominently in all of them.

While ancestral cyanobacteria are assumed to play a central role in Proterozoic biogeochemistry, there is limited direct evidence of the ecological niches that they occupied. The oldest unambiguous cyanobacterial microfossils are found in 2.018- to 2.015-Ga peritidal black cherts of the Orosirian Belcher Group (13, 14). When similarly preserved fossil cyanobacteria are found in younger Proterozoic rocks, they are also interpreted as ancient analogs of benthic cyanobacteria in littoral environments (15). If the paleontological record

is expanded to include all possible microfossils with cyanobacterial affinities, then benthic forms still dominate, with rare and contentious interpretations of cyanobacteria in planktic habitats (16, 17). The lack of fossil indicators for planktic cyanobacteria may reflect an absence of these cyanobacterial lineages at this time (18) or the improbable preservation of cyanobacterial microfossils in pelagic environments (19). Paired biomarker and nitrogen isotope measurements identify the presence of pelagic cyanobacteria by 1.1 Ga ago (20), but earlier documentation of a pelagic habitat would help evaluate hypotheses for the global influence of cyanobacteria in the Proterozoic Earth system.

If Proterozoic cyanobacteria inhabited a globally important ecological niche, the productivity of the biosphere would be largely dependent on their ability to fix carbon. At the level of the global marine ecosystem, the most continuous evidence of carbon fixation by the dominant primary producers is preserved in sedimentary marine carbon isotope records. The carbon isotopic difference between carbonate minerals and total organic carbon (TOC) (ε_{TOC} ; eq. S1) in sedimentary rocks has well-resolved coverage between the GOE, the origin of photosynthetic eukaryotes (21), and the ultimate ecological dominance of photosynthetic eukaryotes in the pelagic marine environment (22). Although the isotopic difference summarized by ε_{TOC} is imparted initially by the net carbon isotope effect associated with carbon fixation by primary producers (ε_p ; eq. S2), carbon isotope fractionations associated with geologic preservation do not allow for ε_{TOC} to be directly substituted for ε_p (23).

We used bootstrap resampling and Monte Carlo simulations to produce a new record of ε_p in the middle of the Proterozoic eon (1.8 to 1.0 Ga ago), taking into account isotopic fractionations that occur as the primary substrates and products of carbon fixation (e.g., dissolved CO_2 and photoautotrophic biomass) are transformed into their final geological states (e.g., carbonate rocks and TOC). This new ε_p record was derived from a curated dataset of carbon isotope measurements from sedimentary rocks from a variety of depositional settings, including open and shallow marine environments (24). The middle Proterozoic shows limited variation in the sedimentary carbon isotope record [e.g., (8, 24)] spanning the proposed “Age of Cyanobacteria” (25). As a result, it represents a favorable target for isolation of any cyanobacterial component of the Proterozoic ε_p record.

Copyright © 2021
The Authors, some
rights reserved;
exclusive licensee
American Association
for the Advancement
of Science. No claim to
original U.S. Government
Works. Distributed
under a Creative
Commons Attribution
NonCommercial
License 4.0 (CC BY-NC).

¹Department of Geological Sciences, University of Colorado Boulder, Boulder, CO 80302, USA. ²Renewable and Sustainable Energy Institute, University of Colorado, Boulder, CO 80309, USA. ³Department of Biochemistry, University of Colorado, Boulder, CO 80309, USA. ⁴National Renewable Energy Laboratory, Golden, CO 80401, USA.

*Corresponding author. Email: sarah.hurley@colorado.edu (S.J.H.); jeffrey.c.cameron@colorado.edu (J.C.C.)

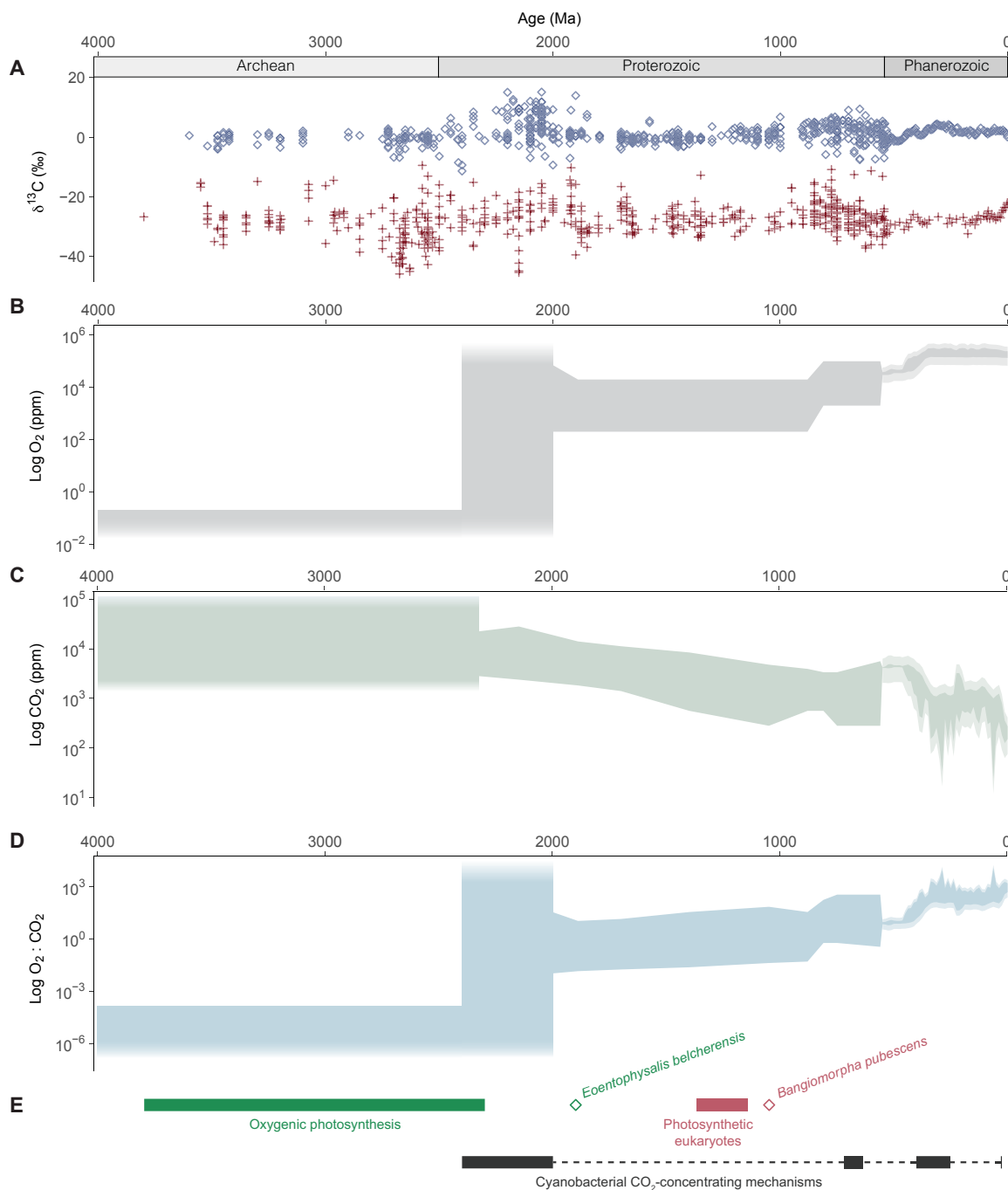


Fig. 1. Isotopic, atmospheric, and biologic context for the Proterozoic “Age of Cyanobacteria” (25). (A) Carbonate $\delta^{13}\text{C}$ values shown in blue diamonds and total organic carbon $\delta^{13}\text{C}$ values shown in red crosses (24). Ma, million years. (B) Mass-independent sulfur isotope fractionation restricts Archean $p\text{O}_2$ estimates to $< 10^{-6}$ PAL or 2 ppm (4). Proterozoic and Phanerozoic $p\text{O}_2$ estimates come from proxies and modeling (8, 59). (C) Archean, Proterozoic, and Phanerozoic CO_2 estimates come from proxies and modeling (8, 39, 59). (D) Estimated range of O_2 -to- CO_2 ratios (each expressed in ppm) from the Archean through the Phanerozoic eons. (E) Range of time estimates for the origin of oxygenic photosynthesis (e.g., 2, 3) shown as a green bar and the earliest unambiguous cyanobacterial microfossils (*Eoentophysalis belcherensis*) shown as a green diamond (13, 14). Age of earliest unambiguous photosynthetic eukaryote (*Bangiomorpha pubescens*) shown as a red diamond with corresponding molecular clock estimates for the primary plastid endosymbiosis shown as a red bar (27). Proposed dates for the emergence of a cyanobacterial CCM shown as black bars [e.g., (34)].

Our statistical simulation of middle Proterozoic ϵ_P values yielded a distribution in which 95% of the values fall between 8 and 24 per mil (‰) (95th percentile) with a median value of 16‰ (Fig. 2A and the SM). This ϵ_P distribution provides a benchmark to compare different autotrophic contributions to global Proterozoic primary production.

Benthic cyanobacteria have, for example, been proposed as ecologically important contributors to Proterozoic primary production (18). In modern cyanobacterial mats, benthic photoautotrophic biomass is commonly enriched in ^{13}C relative to biomass from planktic environments [e.g., (26, 27)]. We used our statistical simulation

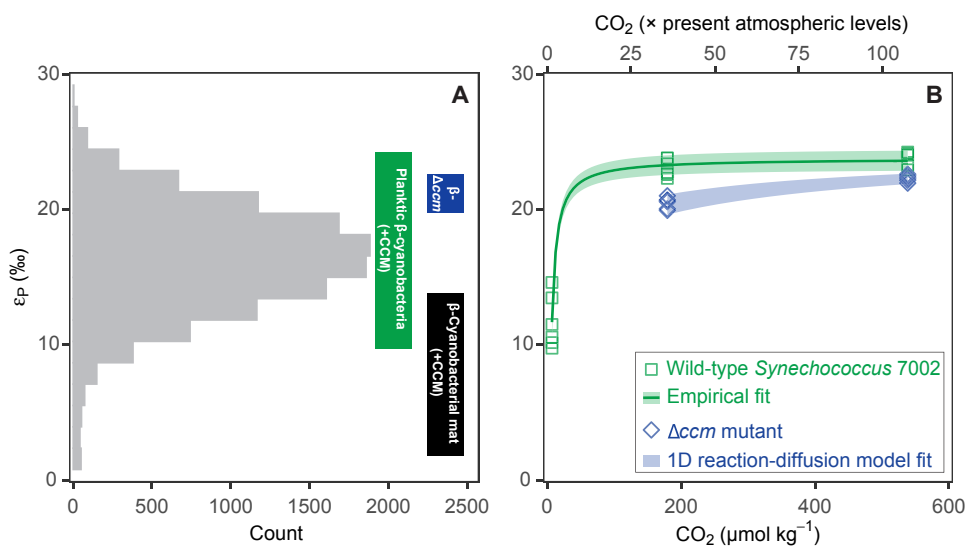


Fig. 2. Middle Proterozoic ϵ_P estimates as compared to empirical cyanobacterial ϵ_P values. (A) Histogram of estimated ϵ_P values between 1.0 and 1.8 Ga. Boxed vertical ranges represent ϵ_P values from a cyanobacterial mat system [black (26)] and ϵ_P values reported here in cultures of WT (green) and Δ_{CCM} mutant (blue) *Synechococcus* sp. PCC 7002 strains. (B) Measured values of ϵ_P increase at higher dissolved CO_2 levels in cultures of *Synechococcus* sp. PCC 7002. In the WT strain (green squares), ϵ_P values covary with $[\text{CO}_{2(\text{aq})}]^{-1}$ (green line, fig. S5; R^2 , 0.96). Blue diamonds are experimental results for the Δ_{CCM} mutant, which requires $\geq 36 \times \text{PAL}$ CO_2 to grow under our experimental conditions. The shaded blue band represents calculations from a 1D reaction-diffusion model trained on physiological observations of the Δ_{CCM} mutant. Horizontal axes refer to CO_2 in the culture headspace relative to PAL (1 PAL = 280 ppm CO_2 ; upper axis) and the corresponding dissolved CO_2 in the culture medium (micromole per kilogram; lower axis). Data points represent biological replicates ($n = 6$ for each condition).

to quantify the distribution of ϵ_P values in a well-characterized modern mat system on the basis of previously published values of $\delta^{13}\text{C}_{\text{carb}}$ and $\delta^{13}\text{C}_{\text{org}}$ (26). In this system, the predicted distribution of ϵ_P values has a median value of 8.5‰ and a range of 4 to 13‰ (95th percentile; fig. S3). This exercise suggests that the dynamics of carbon supply in cyanobacterial mats appears to limit the overall ϵ_P range that they can preserve, especially in hypersaline environments (26). The ϵ_P distribution for this system covers less than 25% of the middle Proterozoic ϵ_P record, with the overlap restricted to a small tail in the Proterozoic distribution that extends to ϵ_P values less than 10‰ (Fig. 2A). Detailed datasets do not exist that can similarly constrain how ϵ_P distributions for cyanobacterial mats might change if CO_2 levels approached those proposed for middle Proterozoic (8). Proof-of-concept experiments, however, indicate that mat ϵ_P values average $\approx 11\text{‰}$ when overlying CO_2 levels are $< 36 \times \text{PAL}$ (1 PAL = 280 ppm CO_2) and approach $\approx 25\text{‰}$ only at CO_2 levels of ≈ 320 to $420 \times \text{PAL}$ [table 2 in (27)]. Although benthic cyanobacterial microfossils are common in the Proterozoic eon, ϵ_P values associated with cyanobacterial mats appear to be much less than those seen in the middle Proterozoic ϵ_P distribution unless CO_2 levels were much greater than proposed for the middle Proterozoic (Fig. 2A).

The middle Proterozoic ϵ_P distribution also differs from ϵ_P values characteristic of planktic cyanobacteria dominant in open ocean ecosystems today (28). Values of ϵ_P cluster from ≈ 15 to 19‰ in physiologically controlled experiments with a planktic member of the monophyletic marine *Synechococcus/Prochlorococcus* (*Syn/Pro*) group (28), *Synechococcus* sp. CCMP838. This tight range spans less than 33% of the middle Proterozoic ϵ_P distribution. Experimental *Syn/Pro* ϵ_P values lack sensitivity to CO_2 levels [between 6 and 18 $\mu\text{mol kg}^{-1}$ (28)] or specific growth rate (28), which suggests that variations in these factors cannot be called on to explain the full middle Proterozoic ϵ_P distribution. A complete interpretation of the Proterozoic carbon isotope record thus seems to require major

contributions by noncyanobacterial primary producers or a shift in our understanding of carbon fixation by Proterozoic cyanobacteria.

It is possible that extant marine cyanobacteria from the *Syn/Pro* clade may not represent apt physiological analogs for Proterozoic cyanobacteria. All extant cyanobacteria use at least one CO_2 -concentrating mechanism (CCM) (29) to increase the supply of CO_2 to rubisco (ribulose 1,5-bisphosphate carboxylase/oxygenase), the key CO_2 -fixing enzyme in the Calvin-Benson cycle (30). Cyanobacterial rubisco is partitioned into a selectively permeable protein microcompartment known as a carboxysome along with carbonic anhydrase. Inside the carboxysome, actively accumulated intracellular HCO_3^- is rapidly interconverted into $\text{CO}_{2(\text{aq})}$ through the activity of carbonic anhydrase (29, 31, 32). Examination of cyanobacterial CCMs reveals a clear division within the phylum (29). The marine *Syn/Pro* clade (α -cyanobacteria) contain α -carboxysomes and Form 1A rubisco that are evolutionarily (29) and structurally distinct (29, 33) from the β -carboxysomes and form 1B rubisco shared by the freshwater, estuarine, and marine species (the β -cyanobacteria) in the remainder of the phylum.

As α -cyanobacteria diverged from cyanobacterial lineages of β -cyanobacteria at the end of the Proterozoic eon, between 1.0 and 0.5 Ga ago (18), β -carboxysomes appear to be the more ancient basis for a cyanobacterial CCM. Estimates for the initial emergence of CCMs in β -cyanobacteria span over 2 Ga of earth history (34) and are often associated with drops in global CO_2 associated with glacial episodes at ca. 2.4 to 2.0 Ga, ca. 0.7 to 0.6 Ga, and, potentially, 0.4 to 0.3 Ga ago (Fig. 1). It is possible that either biochemical differences between α - and β -cyanobacteria or the absence of β -carboxysomes in Proterozoic cyanobacteria could account for the mismatch between ϵ_P values from α -cyanobacteria and the middle Proterozoic ϵ_P distribution. Potential biochemical differences between α - and β -cyanobacteria include the influx and efflux of rubisco substrates

and products from the carboxysome (33) as well the kinetics of rubisco and carbonic anhydrase within the carboxysome (35). These differences would likely alter how whole-cell carbon fixation rates respond to changing environmental conditions (e.g., CO_2 concentrations), potentially expanding or contracting the accessible range of cyanobacterial ε_p values. The possible absence of a β -carboxysome in Proterozoic cyanobacteria would allow freer access of substrates to and from rubisco and carbonic anhydrase, potentially affecting cyanobacterial ε_p values over a wide range of CO_2 concentrations as well.

We propose that primary production by cyanobacteria in the middle Proterozoic might resemble either carbon fixation by extant cyanobacteria with β -carboxysome-based CCMs or a physiologically distinct mode of carbon fixation by ancestral β -cyanobacteria lacking a CCM. To evaluate these possibilities, we determined ε_p values for a model cyanobacterium containing β -carboxysomes, wild-type (WT) *Synechococcus* sp. PCC 7002 (*Synechococcus* 7002), and an engineered mutant of this strain lacking carboxysomes (Δccm) (31, 36, 37) across a range of CO_2 concentrations. Net carbon isotope fractionation by WT *Synechococcus* 7002 allows us to compare ε_p relationships in β -cyanobacteria to previously published ε_p values from α -cyanobacteria (fig. S6) (28). The Δccm mutant, which is high CO_2 requiring, represents a potential physiological analog for pre-CCM-bearing Proterozoic cyanobacteria.

RESULTS

WT *Synechococcus* 7002 grew at dissolved CO_2 concentrations of 7 to 538 $\mu\text{mol l}^{-1}$, corresponding to headspace CO_2 of 1 to 107 \times PAL at pH 6.7 to 8.1. The Δccm mutant failed to grow at CO_2 levels of 1, 18, and 30 \times PAL but was able to grow at 36 and 107 \times PAL at pH 7.3 to 8.1 (fig. S4). These experimental conditions are consistent with both $p\text{CO}_2$ [1 to 100 PAL (8)] and pH [6.8 to 8.2 (38, 39)] estimates relevant to the middle Proterozoic marine biosphere (fig. S10). The ε_p values from acclimated WT batch cultures range from $11.7 \pm 2.0\text{\textperthousand}$ to $23.8 \pm 0.5\text{\textperthousand}$ over 1 to 107 \times PAL, while for Δccm batch cultures, ε_p values range from 20.5 ± 0.4 to 22.3 ± 0.2 over 36 to 107 \times PAL (Fig. 2B). In both the WT and Δccm experiments, values of ε_p increase with higher concentrations of $\text{CO}_{2(\text{aq})}$, in contrast to the insensitivity of ε_p to $\text{CO}_{2(\text{aq})}$ in cyanobacteria with α -carboxysomes (fig. S6A) (28). The positive response of ε_p to increasing CO_2 concentrations indicates that transport limitation is a controlling factor in β -cyanobacterial carbon isotope fractionation, as has been well established for photosynthetic eukaryotes (fig. S6B) (28, 40).

In WT *Synechococcus* 7002, ε_p values show a negative covariation with the inverse of dissolved CO_2 concentrations ($R^2 = 0.96$; figs. S5 and S6), further confirming similarities between cyanobacterial and algal net carbon isotope fractionation. Although the Δccm mutant did not grow over the full range of experimental CO_2 concentrations, it exhibits a 2.5-fold larger decrease in ε_p values over the same drop in CO_2 concentrations when compared to WT ($\approx 1.8\text{\textperthousand}$ versus $\approx 0.7\text{\textperthousand}$ from 107 to 36 \times PAL; Fig. 2B and fig. S5). These different CO_2 responses suggest that different mechanisms control CO_2 transport to rubisco in the Δccm mutant and WT strains.

To explore the isotopic response of the Δccm mutant to varying CO_2 concentrations, we used a one-dimensional (1D) reaction-diffusion model, in which rubisco is uniformly distributed throughout the cytosol (31). This model quantifies the isotopic consequences of the competition between a purely diffusional supply of $\text{CO}_{2(\text{aq})}$ to the site of carbon fixation and CO_2 fixation into biomass, using three

interdependent parameters: (i) the proportion of cellular surface area available for diffusion, (ii) the diffusion coefficient for $\text{CO}_{2(\text{aq})}$ into the cell, and (iii) the distance over which $\text{CO}_{2(\text{aq})}$ diffuses into the cell until it meets a free rubisco and is fixed (see the SM for detailed model description).

Modeled ε_p values for the Δccm mutant increase with respect to CO_2 concentrations (from $\sim 20\text{\textperthousand}$ at 36 \times PAL to $\sim 22\text{\textperthousand}$ at 107 \times PAL) with a slightly nonlinear functional dependence (Fig. 2B). Training the model on measured physiological parameters for the Δccm mutant illustrates the inefficiency of carbon fixation by rubisco relative to a purely diffusional supply of $\text{CO}_{2(\text{aq})}$. To reproduce our ε_p - CO_2 observations, ≈ 70 to 90% of the carbon brought into a cyanobacterium without a carboxysome must be lost through back diffusion. This “leakiness” is calculated as the difference between the gross diffusive flux of CO_2 into the cell and the net rate of CO_2 fixation into biomass. The inability of the Δccm mutant to grow at CO_2 levels below 36 PAL during our experiments (Fig. 2B) was likely due to a combination of factors limiting the intracellular accumulation of CO_2 , including the leakiness of the cell and the lack of an encapsulated carbonic anhydrase to convert accumulated HCO_3^- into CO_2 at the site of carbon fixation.

DISCUSSION

The distribution of ε_p values extracted from the middle Proterozoic sedimentary record span a range of 8 to 24 \textperthousand (95th percentile; Fig. 2A). If cyanobacteria accounted for the majority of primary production at this time, as is commonly asserted, then they should be able to produce a similar range of ε_p values. Our simulations of a previously characterized mat system (26) suggest that net carbon isotope fractionations by cyanobacteria in benthic settings may only account for the lower 25% of the middle Proterozoic ε_p distribution (Fig. 2A). Here, we show that net carbon isotope fractionation by β -cyanobacteria without carboxysomes only covers 13% of the middle Proterozoic ε_p distribution (Fig. 2A). In contrast, the ε_p range that we determined for planktic cyanobacteria with β -carboxysomes covers $>90\%$ of the middle Proterozoic distribution, suggesting that this physiology, in the appropriate ecological niches, could be responsible for a large proportion of Proterozoic primary production (Fig. 2A).

To understand whether evolutionary differences between extant and ancestral rubiscos might allow for β -cyanobacteria without carboxysomes to produce the full middle Proterozoic ε_p range, we used the Δccm model to calculate the ε_p relationships that might characterize β -cyanobacteria lacking carboxysomes with ancestral rubisco under middle Proterozoic CO_2 levels. We incorporated middle Proterozoic estimates of O_2 concentrations [0.1 to 10% PAL, compiled in (8)] in these model simulations as well. Although the timing of evolutionary changes within the rubisco phylogeny remains unconstrained (41), maximum carboxylation rates for ancestral variants of form 1B rubisco are ~ 50 to 70% of their modern equivalents, while the corresponding Menten constants for $\text{CO}_{2(\text{aq})}$ are ~ 40 to 80% of their modern equivalents (42). Over a wide range of dissolved CO_2 and O_2 concentrations relevant to the Proterozoic ocean, our calculations suggest that a cyanobacterium without carboxysomes will exhibit a limited range of whole-cell ε_p values ($<\sim 10\text{\textperthousand}$; Fig. 3 and the SM). While lower O_2 concentrations slightly contract the range of ε_p values (by $\sim 3\%$) relative to those accessible at higher O_2 concentrations, the primary control seems to be the mismatch between a fast rate of

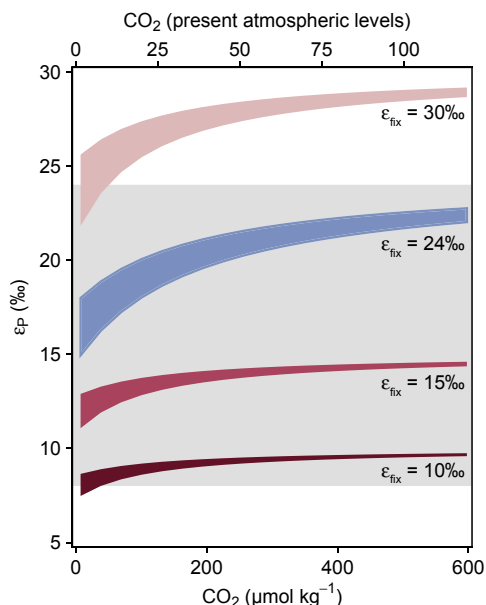


Fig. 3. Modeled relationships between ϵ_P and CO_2 concentration for β -cyanobacteria without a CCM incorporating estimated middle Proterozoic O_2 levels [0.1 to 10% PAL (8)]. The gray band represents the estimated middle Proterozoic distribution of ϵ_P values (95th percentile; 8 to 24‰). The blue field represents calculations extending the observed fractionation by the Δ_{CCM} mutant across possible Proterozoic CO_2 and O_2 levels. The red fields represent calculations incorporating the measured kinetics of ancestral form 1B rubisco (table S3) (42) and the full range of known intrinsic isotope effects for rubisco ($\epsilon_{\text{fix}} = 10, 15, \text{ and } 30\text{\textperthousand}$; the SM).

CO_2 supply by diffusion and a slower rate of CO_2 fixation, which restricts the accessible range of net carbon isotope fractionation across all CO_2 levels in the modeled environment (Fig. 3). In this model, the absolute value of each ϵ_P range is set by the intrinsic carbon isotope fractionation factor assumed for rubisco (ϵ_{fix} ; Fig. 3 and the SM). We note that resurrected forms of ancient rubisco have not yet been isotopically characterized. However, it appears that the lack of carboxysomes, rather than how reconstructed rubiscos ultimately fractionate carbon isotopes, restricts any one example of this physiological state from producing the full middle Proterozoic ϵ_P distribution.

The middle Proterozoic ϵ_P distribution ultimately reflects the interaction between the mode of carbon fixation and CO_2 supply for middle Proterozoic autotrophs. Estimates of middle Proterozoic atmospheric $p\text{CO}_2$ values range from 1 to 100 PAL (8), but the temporal and spatial resolution of these estimates is extremely coarse. The Our middle Proterozoic ϵ_P distribution encompasses a variety of marine environments and atmospheric conditions over the course of 800 million years, and therefore, $p\text{CO}_2$ and dissolved CO_2 could have exhibited wide variation in time and space over this interval. Estimates of $p\text{CO}_2$ over the past ≈ 70 million years, for example, span a relative range of ≈ 150 -fold (60 to 8900 ppm by volume; <https://www.paleo-co2.org>), while dissolved CO_2 in the modern ocean varies over a relative range of ≈ 370 -fold [8 to 2900 $\mu\text{mol kg}^{-1}$ (43)]. If atmospheric or marine CO_2 in the middle Proterozoic varied similarly then planktic cyanobacteria with β -carboxysomes could produce the full range of middle Proterozoic ϵ_P values because of the strong dependence of their net carbon isotope fractionation on CO_2 concentrations (Fig. 2).

Although this inference does not rule out alternate forms of carbon fixation, the ranges of ϵ_P values produced by other plausible middle

Proterozoic primary producers appear to be more restricted even when large variations in middle Proterozoic CO_2 concentrations are considered. In the case of β -cyanobacteria lacking CCMs, this is due to the slow rate of CO_2 fixation relative to the fast supply of CO_2 by diffusion, which restricts the ϵ_P response across different CO_2 concentrations (Fig. 3). Anoxygenic phototrophs lack carboxysomes (44), suggesting that their isotopic fractionation may show a similar lack of sensitivity to CO_2 concentrations as the Δ_{CCM} mutant investigated here. In cyanobacterial mats, limited CO_2 supply appears to restrict ϵ_P to low values except, perhaps, when CO_2 levels are >300 PAL (27). Hypotheses that call on different carbon fixation modes to explain the middle Proterozoic ϵ_P distribution would therefore require the fortuitous preservation of the products of carbon fixation by a diversity of different primary producers.

We recognize that we cannot exclusively rule out these diversity hypotheses, but the genetic, biochemical, environmental, and physiological evidence discussed here points toward a prominent role for ancestral cyanobacteria with β -carboxysome-based CCMs in the middle Proterozoic biosphere. A Paleoproterozoic (or earlier) origin for the CCM in cyanobacteria is consistent with taphonomic inferences of late Mesoproterozoic biomineralization by CCM-bearing cyanobacteria (45). Cyanobacterial CCMs increase the access of rubisco to CO_2 to mitigate the enzyme's dual-substrate specificity for both CO_2 and O_2 [e.g., (46)]. Under the O_2 -to- CO_2 ratios found in modern environments, competition between carboxylation and oxygenation reactions is metabolically expensive and imposes a wasteful loss of fixed carbon (47). Although Proterozoic $p\text{CO}_2$ estimates are higher than modern, spanning ~ 1 to 100 PAL [compiled in (8)], the jump in atmospheric O_2 across the GOE (1, 48) increased the ratio of O_2 to CO_2 up to 100 million-fold (Fig. 1). These enhanced ratios were sustained throughout the Proterozoic at values at least four orders of magnitude greater than at the end of the Archean.

The transition to higher O_2 -to- CO_2 ratios in the Proterozoic marine environment would have increased O_2 -to- CO_2 ratios within Proterozoic cyanobacteria (49). The carboxysome may therefore have been an evolutionary innovation in response to extreme environmental oxygenation across the GOE. Despite being the principal component of the CCM in all cyanobacteria today, the carboxysome's original function may have been to shield rubisco from O_2 (50), after which it was repurposed as a CCM. This proposed function is consistent with predictions of limited CO_2 and O_2 permeation through the central pores of carboxysomal shell proteins (33). Early encapsulation inside of a dysoxic carboxysome could further explain why the specificity for CO_2 versus O_2 is lower in cyanobacterial form 1B rubisco than in form 1B rubisco from Archaeplastida (51), despite a common lineage [e.g., (19)] and over a billion years of shared environmental history (21).

Whether or not the carboxysome originated as an O_2 -exclusion mechanism, its carbon isotope consequences appear to reach back at least 1.8 Ga (Fig. 2). Paleontological interpretations of ancestral cyanobacteria have long been rationalized in terms of morphological and local ecological stasis on geological time scales [e.g., (52)]. The observations reported here extend this working hypothesis of stasis to levels of biological organization—from the global marine ecosystem down to the organellar and, perhaps, biochemical realms—that have not been previously accessible to paleontological insight (17, 19). When viewed in terms of the comprehensive nature of the Proterozoic carbon isotope record, this suggests that, like in the modern ocean, pelagic cyanobacteria were an important component

of Proterozoic marine primary productivity. If Proterozoic cyanobacteria were not strictly benthic forms restricted to littoral environments, then a range of hypotheses for limited primary productivity can be ruled out, from environmental hypotheses that rely on an inaccessible pelagic photic zone (53, 54) to evolutionary hypotheses that posit a planktic lifestyle as a derived trait (18, 55). The possibility that Proterozoic cyanobacteria so closely resembled an extant model cyanobacterium opens the door to direct testing of other hypotheses for limiting primary productivity [e.g., (9–12)] through new experiments in comparative physiology and competition under proposed Proterozoic environmental regimes. Cyanobacterial stasis in terms of ecology, morphology, cytology, and biochemistry may have been the foundation behind low Proterozoic productivity (7). The progressive increase of productivity through time could represent a stepwise scaling (56) away from this continuously maintained cyanobacterial state through the introduction of new avenues of primary production in the oceans (19) and, eventually, on land.

MATERIALS AND METHODS

Middle Proterozoic ϵ_p values

Our statistical simulations were based on bootstrap resampling of a curated dataset of $\delta^{13}\text{C}$ values of carbonate minerals and TOC in 1.0- to 1.8-Ga-old sedimentary rocks (24). We sampled uniform distributions representing possible C isotope fractionation during the conversion and preservation of dissolved CO_2 as carbonate minerals and primary biomass as TOC. The distribution of equilibrium isotope effects between $\text{CO}_{2(\text{aq})}$ and HCO_3^- ($\epsilon_{\text{HCO}_3^--\text{CO}_{2(\text{aq})}}$) ranged from 8.9 to 11.7‰ (57) assuming photic zone temperatures of 3° to 30°C [e.g., (38)]. Experimentally determined kinetic isotope effects associated with the precipitation of calcite and aragonite relative to HCO_3^- ($\epsilon_{\text{cc}-\text{HCO}_3^-}$) ranged from 0.8 to 3.3‰ (58). Carbon isotope fractionations associated with secondary biological processes such as heterotrophic consumption of primary organic matter ($\epsilon_{\text{reworking}}$) ranged from 0 to 1.5‰ (23). Full simulations are detailed in the SM.

Culturing and isotope assays

Synechococcus sp. strain PCC 7002 (*Synechococcus* 7002) and a previously engineered Δccm mutant strain lacking a carboxysome were grown in A+ media, at 37°C under saturating light levels of $\sim 227 \pm 5 \mu\text{mol photons m}^{-2} \text{ s}^{-1}$ provided by cool-white fluorescence lamps. Cultures were grown in 125-ml conical flasks with foam stoppers (Jaece Industries Identi-plug), continuously shaking, in an incubator that kept headspace CO_2 constant by continuous replacement with a mixture of CO_2 and air during each experiment. Headspace CO_2 varied across three experimental conditions: 0.04% (v/v) CO_2 (air), 1% (v/v) CO_2 , and 3% (v/v) CO_2 , corresponding to $\text{CO}_{2(\text{aq})}$ concentrations of 7, 180, and 538 $\mu\text{mol kg}^{-1}$, respectively. At each CO_2 condition, strains were acclimated through the serial inoculation of four consecutive cultures. Each culture grew to an optical density at 730 nm of ~ 0.2 before inoculating the next culture with 1 to 3% of the final cell density and harvesting biomass. Harvested biomass was kept at -70°C , then centrifuged, and washed twice with ultrapurified water before isotopic analysis. Carbon isotope compositions of biomass were determined by first combusting samples in a Thermo Fisher Scientific FlashEA under a flow of He gas. The resultant CO_2 was analyzed with a Thermo Fisher Scientific Delta V Isotope Ratio Mass Spectrometer in continuous-flow mode. Carbon isotope compositions are expressed as the relative per mil difference

between the ratio of $^{13}\text{C}/^{12}\text{C}$ in the sample ($^{13}\text{C}/^{12}\text{C}_{\text{sample}}$) and a standard of Vienna Pee Dee Belemnite ($^{13}\text{C}/^{12}\text{C}_{\text{VPBD}}$). Headspace CO_2 gas was purified and analyzed with a Thermo Fisher Scientific 253+ Isotope Ratio Mass Spectrometer in dual-inlet mode.

One-dimensional reaction-diffusion model

A full model description is in the SM. We used a 1D model of steady-state diffusion of CO_2 between an infinite extracellular source and an intracellular sink to represent rubisco-catalyzed entry of CO_2 into the Calvin-Benson cycle. A fixed distance separates the CO_2 source and enzymatic sink. Both the diffusive transport and the sink reaction are isotopically selective. Independent model inputs include the carbon fixation rates observed for the Δccm mutant grown under 1 and 3% CO_2 headspace, the calculated concentration of dissolved CO_2 , and fractionation factors for form 1B rubisco (ϵ_{fix}) and diffusion of CO_2 in solution (ϵ_{diff}). The model has three free parameters: (i) the intracellular distance over which $\text{CO}_{2(\text{aq})}$ diffuses, (ii) the intracellular diffusion coefficient for $\text{CO}_{2(\text{aq})}$, and (iii) the proportion of cellular surface area available for diffusion. We “trained” the model by selecting interdependent sets of these three parameters that could reproduce experimental ϵ_p values at the observed carbon fixation rates in the Δccm mutant. In the trained model, we additionally used previously characterized kinetics of extant rubiscos and reconstructed ancestral rubiscos to determine possible ϵ_p values in β -cyanobacteria without a CCM over a range of environmental conditions.

SUPPLEMENTARY MATERIALS

Supplementary material for this article is available at <http://advances.sciencemag.org/cgi/content/full/7/2/eabc8998/DC1>

[View/Request a protocol for this paper from Bio-protocol.](#)

REFERENCES AND NOTES

1. D. E. Canfield, The early history of atmospheric oxygen: Homage to Robert M. Garrels. *Annu. Rev. Earth Planet. Sci.* **33**, 1–36 (2005).
2. W. W. Fischer, J. Hemp, J. E. Johnson, Evolution of oxygenic photosynthesis. *Annu. Rev. Earth Planet. Sci.* **44**, 647–683 (2016).
3. P. Sánchez-Baracaldo, T. Cardona, On the origin of oxygenic photosynthesis and Cyanobacteria. *New Phytol.* **225**, 1440–1446 (2020).
4. D. C. Catling, K. J. Zahne, The Archean atmosphere. *Sci. Adv.* **6**, eaax1420 (2020).
5. M. S. W. Hodgeskiss, P. W. Crockford, Y. Peng, B. A. Wing, T. J. Horner, A productivity collapse to end Earth's Great Oxidation. *Proc. Natl. Acad. Sci. U.S.A.* **116**, 17207–17212 (2019).
6. N. J. Planavsky, C. T. Reinhard, X. Wang, D. Thomson, P. McGoldrick, R. H. Rainbird, T. Johnson, W. W. Fischer, T. W. Lyons, Low mid-Proterozoic atmospheric oxygen levels and the delayed rise of animals. *Science* **346**, 635–638 (2014).
7. P. W. Crockford, J. A. Hayles, H. Bao, N. J. Planavsky, A. Bekker, P. W. Fralick, G. P. Halverson, T. H. Bui, Y. Peng, B. A. Wing, Triple oxygen isotope evidence for limited mid-Proterozoic primary productivity. *Nature* **559**, 613–616 (2018).
8. P. W. Crockford, M. Kunzmann, A. Bekker, J. Hayles, H. Bao, G. P. Halverson, Y. Peng, T. H. Bui, G. M. Cox, T. M. Gibson, S. Wörndle, R. Rainbird, A. Lepland, N. L. Swanson-Hysell, S. Master, B. Sreenivas, A. Kuznetsov, V. Krupenik, B. A. Wing, Claypool continued: Extending the isotopic record of sedimentary sulfate. *Chem. Geol.* **513**, 200–225 (2019).
9. M. A. Kipp, E. Stüeken, Biomass recycling and Earth's early phosphorus cycle. *Sci. Adv.* **3**, eaao4795 (2017).
10. S. L. Olson, C. T. Reinhard, T. W. Lyons, Cyanobacterial diazotrophy and Earth's delayed oxygenation. *Front. Microbiol.* **7**, 1526 (2016).
11. C. Scott, T. W. Lyons, A. Bekker, Y. Shen, S. W. Poulton, X. Chu, A. D. Anbar, Tracing the stepwise oxygenation of the Proterozoic ocean. *Nature* **452**, 456–459 (2008).
12. K. Ozaki, K. J. Thompson, R. L. Simister, S. A. Crowe, C. T. Reinhard, An oxygenic photosynthesis and the delayed oxygenation of Earth's atmosphere. *Nat. Commun.* **10**, 3026 (2019).
13. H. J. Hofmann, Precambrian Microflora, Belcher Islands, Canada: Significance and systematics. *J. Paleo.* **50**, 1040–1073 (1976).
14. M. S. W. Hodgeskiss, O. M. J. Dagnaud, J. L. Frost, G. P. Halverson, M. D. Schmitz, N. L. Swanson-Hysell, E. A. Sperling, New insights on the Orosirian carbon cycle, early

Cyanobacteria, and the assembly of Laurentia from the Paleoproterozoic Belcher Group. *Earth Planet. Sci. Lett.* **520**, 141–152 (2019).

15. L. C. Kah, A. H. Knoll, Microbenthic distribution of Proterozoic tidal flats: Environmental and taphonomic considerations. *Geology* **24**, 79–82 (1996).
16. V. N. Sergeev, M. Sharma, Y. Shukla, Proterozoic fossil cyanobacteria. *Palaeobotanist* **61**, 189–358 (2012).
17. C. F. Demoulin, Y. J. Lara, L. Cornet, C. François, D. Baurain, A. Wilmette, E. J. Javaux, Cyanobacteria evolution: Insight from the fossil record. *Free Radic. Biol. Med.* **140**, 206–223 (2019).
18. P. Sánchez-Baracaldo, Origin of marine planktonic cyanobacteria. *Sci. Rep.* **5**, 17418 (2015).
19. A. H. Knoll, R. E. Summons, J. R. Waldbauer, J. E. Zumberge, The geological succession of primary producers in the oceans, in *Evolution of Primary Producers in the Sea* (Elsevier, 2007), pp. 133–163.
20. N. Gueneli, A. M. McKenna, N. Ohkouchi, C. J. Boreham, J. Beghin, E. J. Javaux, J. J. Brocks, 1.1-billion-year-old porphyrins establish a marine ecosystem dominated by bacterial primary producers. *Proc. Natl. Acad. Sci. U.S.A.* **115**, E6978–E6986 (2018).
21. T. M. Gibson, P. M. Shih, V. M. Cumming, W. W. Fischer, P. W. Crockford, M. S. W. Hodgskiss, S. Wörndle, R. A. Creaser, R. H. Rainbird, T. M. Skulski, G. P. Halverson, Precise age of *Bangiomorpha pubescens* dates the origin of eukaryotic photosynthesis. *Geology* **46**, 135–138 (2017).
22. J. J. Brocks, A. J. M. Jarrett, E. Sirantoini, C. Hallmann, Y. Hoshino, T. Liyanage, The rise of algae in Cryogenian oceans and the emergence of animals. *Nature* **548**, 578–581 (2017).
23. J. M. Hayes, H. Strauss, A. J. Kaufman, The abundance of ^{13}C in marine organic matter and isotopic fractionation in the global biogeochemical cycle of carbon during the past 800 Ma. *Chem. Geol.* **161**, 103–125 (1999).
24. J. Krissansen-Totton, R. Buick, D. C. Catling, A statistical analysis of the carbon isotope record from the Archean to Phanerozoic and implications for the rise of oxygen. *Am. J. Sci.* **315**, 275–316 (2015).
25. J. Schopf, M. Walter, in *The Biology of Cyanobacteria*, N. G. Carr, B. A. Whitton, Eds. (Blackwell, 1982), pp. 543–564.
26. M. Schidlowski, H. Gorzawski, I. Dor, Carbon isotope variations in a solar pond microbial mat: Role of environmental gradients as steering variables. *Geochim. Cosmochim. Acta* **58**, 2289–2298 (1994).
27. D. J. Des Marais, D. E. Canfield, The carbon isotope biogeochemistry of microbial mats, in *Microbial Mats: Structure, Development and Environmental Significance*, L. J. Stal, P. Caumette, Eds. (Springer Berlin Heidelberg, 1994), pp. 289–298.
28. B. N. Popp, E. A. Laws, R. R. Bidigare, J. E. Dore, K. L. Hanson, S. G. Wakeham, Effect of phytoplankton cell geometry on carbon isotopic fractionation. *Geochim. Cosmochim. Acta* **62**, 69–77 (1998).
29. B. D. Rae, B. M. Long, M. R. Badger, G. D. Price, Functions, compositions, and evolution of the two types of carboxysomes: Polyhedral microcompartments that facilitate CO_2 fixation in cyanobacteria and some proteobacteria. *Microbiol. Mol. Biol. Rev.* **77**, 357–379 (2013).
30. T. D. Sharkey, Discovery of the canonical Calvin–Benson cycle. *Photosynth. Res.* **140**, 235–252 (2019).
31. J. C. Cameron, S. C. Wilson, S. L. Bernstein, C. A. Kerfeld, Biogenesis of a bacterial organelle: The carboxysome assembly pathway. *Cell* **155**, 1131–1140 (2013).
32. N. C. Hill, J. W. Tay, S. Altus, D. M. Bortz, J. C. Cameron, Life cycle of a cyanobacterial carboxysome. *Sci. Adv.* **6**, eaba1269 (2020).
33. P. Mahinthichaichan, D. M. Morris, Y. Wang, G. J. Jensen, E. Tajkhorshid, Selective permeability of carboxysome shell pores to anionic molecules. *J. Phys. Chem. B* **122**, 9110–9118 (2018).
34. M. Giordano, J. Beardall, J. A. Raven, CO_2 concentrating mechanisms in algae: Mechanisms, environmental modulation, and evolution. *Annu. Rev. Plant Biol.* **56**, 99–131 (2005).
35. L. Whitehead, B. M. Long, G. D. Price, M. R. Badger, Comparing the in vivo function of α -carboxysomes and β -carboxysomes in two model cyanobacteria. *Plant Physiol.* **165**, 398–411 (2014).
36. G. C. Gordon, T. C. Korosh, J. C. Cameron, A. L. Markley, M. B. Begemann, B. F. Pfleger, CRISPR interference as a titratable, *trans*-acting regulatory tool for metabolic engineering in the cyanobacterium *Synechococcus* sp. strain PCC 7002. *Metab. Eng.* **38**, 170–179 (2016).
37. R. L. Clark, G. C. Gordon, N. R. Bennett, H. Lyu, T. W. Root, B. F. Pfleger, High- CO_2 requirement as a mechanism for the containment of genetically modified cyanobacteria. *ACS Synth. Biol.* **7**, 384–391 (2018).
38. J. Krissansen-Totton, G. N. Arney, D. C. Catling, Constraining the climate and ocean pH of the early Earth with a geological carbon cycle model. *Proc. Natl. Acad. Sci.* **115**, 4105–4110 (2018).
39. I. Halevy, A. Bachan, The geologic history of seawater pH. *Science* **355**, 1069–1071 (2017).
40. E. A. Laws, B. N. Popp, R. R. Bidigare, M. C. Kennicutt, S. A. Macko, Dependence of phytoplankton carbon isotopic composition on growth rate and $[\text{CO}_2]_{\text{aq}}$: Theoretical considerations and experimental results. *Geochim. Cosmochim. Acta* **59**, 1131–1138 (1995).
41. B. Kacar, V. Hanson-Smith, Z. R. Adam, N. Boekelheide, Constraining the timing of the Great Oxidation Event within the Rubisco phylogenetic tree. *Geobiology* **15**, 628–640 (2017).
42. P. M. Shih, A. Occhialini, J. C. Cameron, P. J. Andralojc, M. A. J. Parry, C. A. Kerfeld, Biochemical characterization of predicted Precambrian RuBisCO. *Nat. Commun.* **7**, 10382 (2016).
43. M. Lebrero, D. Garbe-Schönberg, M. N. Müller, S. Blanco-Ameijeiras, R. A. Feely, L. Lorenzoni, J.-C. Molinero, K. Bremer, D. O. B. Jones, D. Iglesias-Rodríguez, D. Greeley, M. D. Lamare, A. Paulmier, M. Graco, J. Cartes, J. Barcelos e Ramos, A. de Lara, R. Sanchez-Leal, P. Jimenez, F. E. Paparazzo, S. E. Hartman, U. Westernströer, M. Küter, R. Benavides, A. F. da Silva, S. Bell, C. Payne, S. Olafsdottir, K. Robinson, L. M. Jantunen, A. Koralev, R. J. Webster, E. M. Jones, O. Gilg, P. B. du Bois, J. Beldowski, C. Ashjian, N. D. Yahia, B. Twining, X.-G. Chen, L.-C. Tseng, J.-S. Hwang, H.-U. Dahms, A. Oschlies, Global variability in seawater Mg/Ca and Sr/Ca ratios in the modern ocean. *Proc. Natl. Acad. Sci. U.S.A.* **117**, 22281–22292 (2020).
44. K.-H. Tang, Y. Tang, R. E. Blankenship, Carbon metabolic pathways in phototrophic bacteria and their broader evolutionary implications. *Front. Microbiol.* **2**, 165 (2011).
45. L. C. Kah, R. Ridings, Mesoproterozoic carbon dioxide levels inferred from calcified cyanobacteria. *Geology* **35**, 799–802 (2007).
46. G. D. Price, M. R. Badger, F. J. Woodger, B. M. Long, Advances in understanding the cyanobacterial CO_2 -concentrating-mechanism (CCM): Functional components, CO_2 transporters, diversity, genetic regulation and prospects for engineering into plants. *J. Exp. Bot.* **59**, 1441–1461 (2008).
47. H. Bauwe, M. Hagemann, A. R. Fernie, Photorespiration: Players, partners and origin. *Trends Plant Sci.* **15**, 330–336 (2010).
48. A. Bachan, L. R. Kump, The rise of oxygen and siderite oxidation during the Lomagundi Event. *Proc. Natl. Acad. Sci. U.S.A.* **112**, 6562–6567 (2015).
49. S. Kihara, D. A. Hartzler, S. Savikhin, Oxygen concentration inside a functioning photosynthetic cell. *Biophys. J.* **106**, 1882–1889 (2014).
50. G. C. Cannon, C. E. Bradburne, H. C. Aldrich, S. H. Baker, S. Heinhorst, J. M. Shively, Microcompartments in prokaryotes: Carboxysomes and related polyhedra. *Appl. Environ. Microbiol.* **67**, 5351–5361 (2001).
51. A. I. Flamholz, N. Prywes, U. Moran, D. Davidi, Y. M. Bar-On, L. M. Oltrogge, R. Alves, D. Savage, R. Milo, Revisiting trade-offs between Rubisco kinetic parameters. *Biochemistry* **58**, 3365–3376 (2019).
52. J. W. Schopf, Disparate rates, differing fates: Tempo and mode of evolution changed from the Precambrian to the Phanerozoic. *Proc. Natl. Acad. Sci. U.S.A.* **91**, 6735–6742 (1994).
53. E. D. Swanner, A. M. Młoszewska, O. A. Cirkpa, R. Schoenberg, K. O. Konhauser, A. Kappler, Modulation of oxygen production in Archaean oceans by episodes of $\text{Fe}(\text{II})$ toxicity. *Nat. Geosci.* **8**, 126–130 (2015).
54. A. M. Młoszewska, D. B. Cole, N. J. Planavsky, A. Kappler, D. S. Whitford, G. W. Owttrim, K. O. Konhauser, UV radiation limited the expansion of cyanobacteria in early marine photic environments. *Nat. Commun.* **9**, 3088 (2018).
55. G. J. Dick, S. L. Grim, J. M. Klatt, Controls on O_2 production in cyanobacterial mats and implications for Earth's oxygenation. *Annu. Rev. Earth Planet. Sci.* **46**, 123–147 (2018).
56. A. H. Knoll, R. K. Bambach, Directionality in the history of life: Diffusion from the left wall or repeated scaling of the right? *Paleobiology* **26**, 1–14 (2000).
57. J. Zhang, P. D. Quay, D. O. Wilbur, Carbon isotope fractionation during gas–water exchange and dissolution of CO_2 . *Geochim. Cosmochim. Acta* **59**, 107–114 (1995).
58. C. S. Romanek, E. L. Grossman, J. W. Morse, Carbon isotopic fractionation in synthetic aragonite and calcite: Effects of temperature and precipitation rate. *Geochim. Cosmochim. Acta* **56**, 419–430 (1992).
59. T. M. Lenton, S. J. Daines, B. J. W. Mills, COPSE reloaded: An improved model of biogeochemical cycling over Phanerozoic time. *Earth Sci. Rev.* **178**, 1–28 (2018).
60. A. P. Gumsley, K. R. Chamberlain, W. Bleeker, U. Söderlund, M. O. de Kock, E. R. Larsson, A. Bekker, Timing and tempo of the Great Oxidation Event. *Proc. Natl. Acad. Sci.* **114**, 18111–18116 (2017).
61. C. J. Bjerrum, D. E. Canfield, Ocean productivity before about 1.9 Gyr ago limited by phosphorus adsorption onto iron oxides. *Nature* **417**, 159–162 (2002).
62. K. Fennel, M. Follows, P. G. Falkowski, The co-evolution of the nitrogen, carbon and oxygen cycles in the Proterozoic ocean. *Am. J. Sci.* **305**, 526–545 (2005).
63. A. D. Anbar, A. H. Knoll, Proterozoic ocean chemistry and evolution: A Bioinorganic bridge? *Science* **297**, 1137–1142 (2002).
64. D. T. Johnston, F. Wolfe-Simon, A. Pearson, A. H. Knoll, Anoxygenic photosynthesis modulated Proterozoic oxygen and sustained Earth's middle age. *Proc. Natl. Acad. Sci.* **106**, 16925–16929 (2009).
65. N. J. Butterfield, Oxygen, animals and oceanic ventilation: An alternative view. *Geobiology* **7**, 1–7 (2009).
66. P. Sánchez-Baracaldo, A. Ridgwell, J. A. Raven, A Neoproterozoic transition in the marine nitrogen cycle. *Curr. Biol.* **24**, 652–657 (2014).

67. T. L. Hamilton, D. A. Bryant, J. L. Macalady, The role of biology in planetary evolution: Cyanobacterial primary production in low-oxygen Proterozoic oceans. *Environ. Microbiol.* **18**, 325–340 (2016).

68. J. F. Allen, B. Thake, W. F. Martin, Nitrogenase inhibition limited oxygenation of Earth's proterozoic atmosphere. *Trends Plant Sci.* **24**, 1022–1031 (2019).

69. R. E. Summons, J. M. Hayes, Principles of molecular and isotopic biogeochemistry, in *The Proterozoic Biosphere, a Multidisciplinary Study*, J. W. Schopf, C. Klein, Eds. (Cambridge Univ. Press, 1992), pp. 83–94.

70. S. E. Stevens Jr., C. O. P. Patterson, J. Myers, The production of hydrogen peroxide by blue-green algae: A survey¹. *J. Phycol.* **9**, 427–430 (1973).

71. R. E. Zeebe, D. Wolf-Gladrow, *CO₂ in Seawater: Equilibrium, Kinetics, Isotopes* (Oceanography Series, Elsevier, ed. 1, 2001), vol. 65.

72. C. G. Trick, S. W. Wilhelm, Physiological changes in the coastal marine cyanobacterium *Synechococcus* sp. PCC 7002 exposed to low ferric ion levels. *Mar. Chem.* **50**, 207–217 (1995).

73. R. D. Guy, M. L. Fogel, J. A. Berry, Photosynthetic fractionation of the stable isotopes of oxygen and carbon. *Plant Physiol.* **101**, 37–47 (1993).

74. D. B. McNevin, M. R. Badger, S. M. Whitney, S. von Caemmerer, G. G. B. Tcherkez, G. D. Farquhar, Differences in carbon isotope discrimination of three variants of D-ribulose-1,5-bisphosphate carboxylase/oxygenase reflect differences in their catalytic mechanisms. *J. Biol. Chem.* **282**, 36068–36076 (2007).

75. R. L. Clark, J. C. Cameron, T. W. Root, B. F. Pfleger, Insights into the industrial growth of cyanobacteria from a model of the carbon-concentrating mechanism. *AIChE J.* **60**, 1269–1277 (2014).

76. P. J. Thomas, A. J. Boller, S. Satagopan, F. R. Tabita, C. M. Cavanaugh, K. M. Scott, Isotope discrimination by form IC RubisCO from *Ralstonia eutropha* and *Rhodobacter sphaeroides*, metabolically versatile members of 'Proteobacteria' from aquatic and soil habitats. *Environ. Microbiol.* **21**, 72–80 (2019).

77. E. B. Wilkes, A. Pearson, A general model for carbon isotopes in red-lineage phytoplankton: Interplay between unidirectional processes and fractionation by RubisCO. *Geochim. Cosmochim. Acta* **265**, 163–181 (2019).

78. R. E. Zeebe, On the molecular diffusion coefficients of dissolved CO₂, HCO₃[−], and CO₃^{2−} and their dependence on isotopic mass. *Geochim. Cosmochim. Acta* **75**, 2483–2498 (2011).

79. M. H. O'Leary, Measurement of the isotope fractionation associated with diffusion of carbon dioxide in aqueous solution. *J. Phys. Chem.* **88**, 823–825 (1984).

Acknowledgments: We thank E. Ellison, P. Crockford, and E. Johnson for valuable discussions, J. Jackson and R. Dunbar for editorial handling, and five anonymous reviewers for thoughtful comments. We acknowledge B. Davidheiser-Kroll of the CUBES-SIL for assistance with stable isotope analyses and data reduction. **Funding:** This work was supported by an Agouron Institute postdoctoral fellowship to S.J.H., start-up funding from CU Boulder to B.A.W. and J.C.C., NSF-EF1724393 to B.A.W., NIH T32-GM008759 to N.C.H., and by the U.S. Department of Energy (DOE) DE-SC0019306 to J.C.C. **Author contributions:** S.J.H., B.A.W., and J.C.C. designed the study. S.J.H., C.E.J., and N.C.H. performed the research. S.J.H. and B.A.W. wrote the manuscript with contributions from all authors. **Competing interests:** The authors declare that they have no competing interests. **Data and materials availability:** All data needed to evaluate the conclusions in the paper are present in the paper and/or the Supplementary Materials.

Submitted 20 May 2020

Accepted 11 November 2020

Published 6 January 2021

10.1126/sciadv.abc8998

Citation: S. J. Hurley, B. A. Wing, C. E. Jasper, N. C. Hill, J. C. Cameron, Carbon isotope evidence for the global physiology of Proterozoic cyanobacteria. *Sci. Adv.* **7**, eabc8998 (2021).

Carbon isotope evidence for the global physiology of Proterozoic cyanobacteria

Sarah J. Hurley, Boswell A. Wing, Claire E. Jasper, Nicholas C. Hill and Jeffrey C. Cameron

Sci Adv 7 (2), eabc8998.
DOI: 10.1126/sciadv.abc8998

ARTICLE TOOLS

<http://advances.science.org/content/7/2/eabc8998>

SUPPLEMENTARY MATERIALS

<http://advances.science.org/content/suppl/2021/01/04/7.2.eabc8998.DC1>

REFERENCES

This article cites 74 articles, 24 of which you can access for free
<http://advances.science.org/content/7/2/eabc8998#BIBL>

PERMISSIONS

<http://www.science.org/help/reprints-and-permissions>

Use of this article is subject to the [Terms of Service](#)

Science Advances (ISSN 2375-2548) is published by the American Association for the Advancement of Science, 1200 New York Avenue NW, Washington, DC 20005. The title 'Science Advances' is a registered trademark of AAAS.

Copyright © 2021 The Authors, some rights reserved; exclusive licensee American Association for the Advancement of Science. No claim to original U.S. Government Works. Distributed under a Creative Commons Attribution NonCommercial License 4.0 (CC BY-NC).

advances.sciencemag.org/cgi/content/full/7/2/eabc8998/DC1

Supplementary Materials for

Carbon isotope evidence for the global physiology of Proterozoic cyanobacteria

Sarah J. Hurley*, Boswell A. Wing, Claire E. Jasper, Nicholas C. Hill, Jeffrey C. Cameron*

*Corresponding author. Email: sarah.hurley@colorado.edu (S.J.H.); jeffrey.c.cameron@colorado.edu (J.C.C.)

Published 6 January 2021, *Sci. Adv.* 7, eabc8998 (2021)
DOI: 10.1126/sciadv.abc8998

This PDF file includes:

Sections S1 to S7

Figs. S1 to S10

Tables S1 to S3

References

Supplementary Materials

1. Estimates of O₂, CO₂, and oxygenic productivity through Earth history

In broad brush, the concentration of atmospheric oxygen has increased through Earth history in two steps (Fig. S1). Atmospheric oxygen was negligible in the Archean Eon at $<10^{-6}$ preindustrial atmospheric levels (PAL = 280 ppm CO₂ and 200,000 ppm O₂) (4). The Paleoproterozoic accumulation of atmospheric oxygen, the Great Oxidation Event (GOE), was underway by 2.43 Ga, and continued for another \approx 200 million years (60). Atmospheric oxygen concentrations may have reached near modern levels early in the Paleoproterozoic Era at $\sim 10^{-3}$ PAL before returning to values between $\sim 10^{-3}$ to $\sim 10^{-1}$ PAL in the Mesoproterozoic Era (e.g., 1, 4, 8, 61). After land plants arose early in the Paleozoic Era, atmospheric oxygen concentrations increased again from 10^{-1} PAL to approximately present levels with some minor variation afterward (59). In contrast, atmospheric CO₂ concentrations have decreased, perhaps less dramatically, through time. Archean atmospheric CO₂ concentrations of ~ 40 -400 PAL are consistent with atmospheric and general circulation models (7, 8, 39). CO₂ levels declined from potentially ~ 10 -100 PAL at the beginning of the Proterozoic Eon to ~ 1 -20 PAL at the end of the Proterozoic (8). During the Phanerozoic Eon, modeling predicts a general negative covariation in CO₂ concentrations with O₂ concentrations (59).

Environmental, ecological and evolutionary mechanisms have been hypothesized to limit the oxygenic productivity of the marine biosphere on geologic timescales. Some environmental explanations propose nutrient limitation either by phosphorus (9, 62), nitrogen (10, 63), or trace metals (11, 64). Others call on cyanobacterial exclusion from a toxic marine photic zone (53, 54). In ecological scenarios, ecosystem structure is proposed to control oxygen production. Competition between populations of oxygenic and anoxygenic photosynthesizers may have limited oxygenic productivity in the water column

(12, 65). Self-shading within a turbid community of cyanobacteria could have a similar effect on net primary productivity (66). Evolutionary hypotheses ascribe limited oxygenic productivity in the Proterozoic to cyanobacteria with enzymatic (67), metabolic (68), cytological (69), or lifestyle (18, 55) traits of their modern descendants. Although ancestral cyanobacteria play a central role in all potential hypotheses for restricting Proterozoic primary productivity, the geologic record contains limited direct evidence for either their global ecological niche or their intracellular physiology at this time.

2. Estimates of Mid-Proterozoic ε_P values by statistical simulation

Statistical simulations provide a way to extract estimated values of ε_P , the isotopic fractionation between dissolved CO₂ and biomass produced via photoautotrophic carbon fixation, from the geologic carbon isotope record. We restricted our analysis to the non-transitional middle Proterozoic interval (1.0-1.8 Ga), identified previously with a mean difference method (24), to reduce the confounding effects of non-steady state variation in the carbon isotope record. The entire middle Proterozoic interval was treated as a single time bin as finer time-binning did not affect the results of the statistical analysis (24).

We resampled $\delta^{13}\text{C}$ values from a previously published, curated dataset (24). In this dataset, middle Proterozoic carbonates from a variety of depositional settings, including open and shallow marine environments, have homogeneous $\delta^{13}\text{C}$ values with a mean and standard deviation of $0 \pm 1.5 \text{ ‰}$ (Fig. S2). This homogeneity likely reflects the geographically uniform nature of the marine bicarbonate reservoir (70). Total organic carbon measurements in this dataset similarly reflect a broad range of marine environments and were filtered to exclude demonstrably authigenic and, importantly (70), thermally altered sediments (24).

Values of ε_{TOC} , the carbon isotopic fractionation between carbonate minerals ($\delta^{13}\text{C}_{\text{carb}}$) and total organic carbon ($\delta^{13}\text{C}_{\text{org}}$) preserved in the sedimentary rocks (24) is defined as:

$$(1) \quad \varepsilon_{\text{TOC}} \equiv \delta^{13}\text{C}_{\text{carb}} - \delta^{13}\text{C}_{\text{org}},$$

where $\delta^{13}\text{C}_{\text{carb}} = [({}^{13}\text{C}/{}^{12}\text{C}_{\text{carb}})/({}^{13}\text{C}/{}^{12}\text{C}_{\text{standard}}) - 1] * 1000$ and $\delta^{13}\text{C}_{\text{org}} = [({}^{13}\text{C}/{}^{12}\text{C}_{\text{org}})/({}^{13}\text{C}/{}^{12}\text{C}_{\text{standard}}) - 1] * 1000$, both expressed as permil (‰). Bootstrap resampling of middle Proterozoic carbon isotope records yields an ε_{TOC} distribution with a mean of 28 ‰ and a range of $20\text{--}35 \text{ ‰}$ (95th percentile; Fig. S2). ε_{TOC} values represent the combined effects of a number of processes including *i*) the fractionation between dissolved CO₂ and the biomass of primary producers (ε_P), *ii*) the fractionation between dissolved CO₂ and carbonate minerals ($\varepsilon_{\text{HCO}_3^--\text{CO}_2 \text{ (aq)}}$, $\varepsilon_{\text{cal/ara}-\text{HCO}_3^-}$), *iii*) and the fractionation associated with biological reworking of

organic carbon during export and burial ($\varepsilon_{\text{reworking}}$) (23). The isotopic difference between dissolved $\text{CO}_2_{(\text{aq})}$ and biomass produced via photoautotrophic carbon fixation (ε_{P}) is typically defined by:

$$(2) \quad \varepsilon_{\text{P}} = \delta^{13}\text{C}_{\text{CO}_2_{(\text{aq})}} - \delta^{13}\text{C}_{\text{biomass}}.$$

We randomly sampled uniform distributions representing fractionation during the conversion and preservation of dissolved CO_2 as carbonate rocks and primary biomass as TOC. The distribution of equilibrium isotope effects between $\text{CO}_2_{(\text{aq})}$ and HCO_3^- ($\varepsilon_{\text{HCO}_3^- - \text{CO}_2_{(\text{aq})}}$) ranged from 8.9-11.7‰ (57) assuming photic zone temperatures of 3-30°C (e.g., 38). Experimentally determined kinetic isotope effects associated with the precipitation of calcite and aragonite from HCO_3^- ($\varepsilon_{\text{cal/ara-HCO}_3^-}$) ranged from 0.8-3.3‰ (58). Fractionations associated with secondary biological processes such as heterotrophic consumption of primary organic matter ($\varepsilon_{\text{reworking}}$) ranged from 0-1.5‰ (23) (Fig. S2). Values of $\delta^{13}\text{C}$ for dissolved $\text{CO}_2_{(\text{aq})}$ and biomass were calculated according to the following approximations:

$$(3) \quad \delta^{13}\text{C}_{\text{CO}_2_{(\text{aq})}} = \delta^{13}\text{C}_{\text{carb}} - \varepsilon_{\text{cal/ara-HCO}_3^-} - \varepsilon_{\text{HCO}_3^- - \text{CO}_2_{(\text{aq})}}$$

$$(4) \quad \delta^{13}\text{C}_{\text{biomass}} = \delta^{13}\text{C}_{\text{org}} - \varepsilon_{\text{reworking}}$$

The resulting distribution of ε_{P} values, calculated according to Eq. 2, are offset from the ε_{TOC} distribution by ≈12‰, with a mean of 16‰ and a 2 σ range of 8-24‰ (Fig. S2). The statistical simulations were run over 10,000 bootstrap trials.

3. Estimates of modern mat ε_{P} values by statistical simulation

We additionally used these techniques to estimate ε_{P} values from a published characterization of a modern cyanobacterial mat system (26). This mat system was grown and sampled in an experimental pond with a depth of <1 m. The pond was artificially stratified with an anoxic bottom layer of highly concentrated brine and an upper layer diluted with freshwater. We used the same conversion to calculate $\delta^{13}\text{C}_{\text{CO}_2_{(\text{aq})}}$ values from observed $\delta^{13}\text{C}_{\text{carb}}$ values, drawing from uniform distributions representing $\varepsilon_{\text{HCO}_3^- - \text{CO}_2_{(\text{aq})}}$ at observed pond temperatures of 23-57°C and $\varepsilon_{\text{cal/ara-HCO}_3^-}$ (58) (Eq. 3; see previous section for full simulation description). We did not include fractionations associated with secondary biological processes ($\varepsilon_{\text{reworking}}$) due to the young age of the mat, the anoxic bottom layer, and absence of burial in the system. However, due to the small range of $\varepsilon_{\text{reworking}}$ (0-1.5‰), the resulting distribution is relatively insensitive to this

parameter. Statistical simulations of carbon isotope fractionation in this previously characterized mat system yielded an ε_P distribution with a range of 4-13‰ (95th percentile) and a median value of 8.5‰ (Fig. S3), likely reflecting the impact of limited carbon transport into this hypersaline environment.

4. Culturing Description

Culturing experiments used wild-type (WT) *Synechococcus* sp. strain PCC 7002 (*Synechococcus* 7002) and a Δccm mutant strain lacking a carboxysome. The Δccm strain was generated by transforming WT cells in exponential growth phase with 0.5 ng/mL of plasmid DNA, containing a kanamycin resistance cassette flanked by 750 bp homology arms for recombination into the *ccm* locus (36). After incubation at 30°C in constant illumination (~150 µmols photons m⁻² s⁻¹) for 24 hours, transformed cells were selected for with 100 µg/mL kanamycin on A+ media solidified with Bacto Agar (1%; w/v) in 3% (v/v) CO₂. Individual colonies were patched onto new plates and tested for segregation by PCR, using primer pairs specific to either the transformed (primers KAMo0113 and EBJp0048) or WT (primers EBJp0048 and EBJp0006) genome. Presence of the PCR product specific to the transformed genome and absence of the PCR product specific to the WT genome was used as an indicator of full segregation. The 5'-3' sequences for primers are

KAMo0113: CGACTGAATCCGGTGAGAAT,

EBJp0048: CGGTGGAGACGATGATCCG,

and EBJp0006: ATAGGTTCTGAATTGTTCTACTTCTTCGGTGT.

For experiments on carbon isotope fractionation, all cultures grew in A+ media (71) at 37°C under saturating light levels of $\sim 227 \pm 5$ µmol photons m⁻² s⁻¹ provided by cool-white fluorescence lamps.

Cultures were grown in 125 ml conical flasks with foam stoppers (Jaece Industries IdentiplugTM), continuously shaking, in an incubator that kept headspace CO₂ constant by continuous replacement with a mixture of CO₂ and air during each experiment. Headspace CO₂ varied across three experimental conditions: 0.04% (v/v) CO₂, 1% (v/v) CO₂, and 3% (v/v) CO₂, corresponding to CO_{2(aq)} concentrations of 7, 180, and 538 µmol kg⁻¹, respectively. The measured pH of the cultures (8.1 in air, 7.3 in 1% CO₂, and 6.7 in 3% CO₂) and the headspace *p*CO₂ were used to calculate dissolved CO₂ via the csyS program (72) adapted for the R statistical computing environment. Dissolved CO₂ concentrations calculated for the growth medium ranged from 7 µmol kg⁻¹ in air (1× PAL) to 538 µmol kg⁻¹ in 3% CO₂ (107 × PAL). We plot both headspace CO₂ levels and dissolved CO₂ concentrations due to the influence of temperature, salinity, and pH on dissolved CO₂ concentrations.

We attempted to grow the Δccm mutant lacking carboxysomes at both 0.5% (v/v) and 0.8% (v/v) CO₂, corresponding to 18 × PAL and 30 × PAL. However, under our experimental conditions, the mutant strain was only able to grow at 1% CO₂ (36 × PAL) or greater, consistent with the previously observed

inability of this high-CO₂-requiring phenotype to grow in air (31). Strains were acclimated to each CO₂ condition over the course of four serially-transferred cultures. Cultures grew to an OD_{730 nm} of ~0.2 before inoculating the next acclimation with 1-3% of the final cell density and harvesting biomass (Fig. S4). Harvested biomass was kept at -70°C. Prior to isotopic analysis, biomass was centrifuged and washed twice with ultrapurified water.

For cultures, values of ε_P were calculated relative to external $\delta^{13}\text{C}$ values for CO_{2(aq)} according to:

$$(5) \quad \varepsilon_P = 1000 \left[\frac{(\delta^{13}\text{C}_{\text{CO}_2(\text{aq})} + 1000)}{(\delta^{13}\text{C}_{\text{biomass}} + 1000)} - 1 \right]$$

The net specific growth rate of each culture, μ (h⁻¹), was calculated according to:

$$(6) \quad \mu = \frac{\ln(\text{cell density}_{\text{final}}) - \ln(\text{cell density}_{\text{initial}})}{(t_{\text{final}} - t_{\text{initial}})}$$

Initial or final cell densities are in cells ml⁻¹ and $t_{\text{final}} - t_{\text{initial}}$ is the duration of each batch culture in hours. Carbon fixation rates (μg C cell⁻¹ s⁻¹) were calculated by multiplying the carbon content per cell (μg C cell⁻¹) by the net specific growth rate in s⁻¹:

$$(7) \quad C_{\text{fix}} = C_{\text{cell}} \cdot \mu$$

Growth parameters for all cultures are plotted in Fig. S5 and reported in Table S1. Doubling times for the wild-type strain ranged from 5.1 ± 0.7 h grown under air, 3.6 ± 0.6 h grown under 1% CO₂ and 4.0 ± 0.3 h grown under 3% CO₂ on average. Doubling times for the Δccm mutant grown under equivalent headspaces were slightly greater (slower growth rates) under 1% CO₂ (5.5 ± 1.0 h) and slightly smaller (faster growth rates) under 3% CO₂ (3.5 ± 0.7 h). Carbon fixation rates for the wild-type strain were 67 ± 21, 98 ± 36, and 106 ± 30 fg C cell⁻¹ h⁻¹ grown under air, 1%, and 3% CO₂, respectively (Table S1). Carbon fixation rates for the Δccm mutant were 105 ± 33 and 166 ± 44 fg C cell⁻¹ h⁻¹ grown under 1% and 3% CO₂, respectively. The carbon fixation rates for wild-type strain in air (67 ± 21 fg C cell⁻¹ h⁻¹) are ~3× previously published carbon fixation rates for *Synechococcus* 7002 (73).

5. Carbon isotope measurements

The carbon isotope composition of cyanobacterial biomass was measured in the Earth Systems Stable Isotope Lab at the University of Colorado Boulder. Samples were oxidized and combusted with a

Thermo Scientific FlashEA and the resultant CO₂ was analyzed with a Thermo Scientific Delta V Isotope Ratio Mass Spectrometer. Ratios are expressed as ¹³C/¹²C in units of relative per mil (‰) difference between the sample (R_{sample}) and a standard (R_{standard}) of Vienna PeeDee Belemnite (VPDB) according to:

$$(8) \quad \delta^{13}\text{C} = [({}^{13}\text{C}/{}^{12}\text{C}_{\text{sample}}/{}^{13}\text{C}/{}^{12}\text{C}_{\text{standard}}) - 1] * 1000 \text{ (‰)}$$

Acetanilide (University of Indiana; δ¹³C of -29.53‰; weight % C of 71.09) was used to correct for linearity and drift. Acetanilide was additionally used as a monitoring standard and a bovine gelatin (pugel), from University of California Santa Cruz (δ¹³C of -12.62‰; weight % C 44.02) as a discrimination standard.

Isotopic analysis of CO₂ gas was conducted in the Earth Systems Stable Isotope Lab at the University of Colorado Boulder. The CO₂ was analyzed with a Thermo Scientific 253+ Isotope Ratio Mass Spectrometer. The gas was analyzed for four runs with seven cycles at 12.5 volts on 44 m/z with an integration time of 26 s per cycle. Ratios are expressed as ¹³C/¹²C in units of relative per mil (‰) difference between the sample (R_{sample}) and a standard (R_{standard}) of VPBD. The gas was run against an in-house standard that has been corrected against several commercially purchased Oztec bottles of varying compositions.

6. 1D reaction-diffusion model

We used a one-dimensional (1D) model of steady-state diffusion of CO₂ between an infinite source and a sink to represent rubisco-catalyzed entry of CO₂ into the Calvin-Benson cycle (Fig. S7). A fixed distance, L, separates the CO₂ source and enzymatic sink. Both diffusion and the sink reaction are isotopically selective according to $\varepsilon_{\text{diffusion}}$ and ε_{fix} , respectively (Table S2). Here, ε_{fix} refers to the kinetic fractionation factor associated with rubisco (= $\varepsilon_{\text{rubisco}}$). Steady-state diffusion in 1D is described by:

$$(9) \quad D \times \frac{d^2C}{dz^2} = 0,$$

where D is the diffusion coefficient, C is the concentration of dissolved CO₂ ($= {}^{13}\text{CO}_2 + {}^{12}\text{CO}_2$), and z is the distance coordinate between source and sink. Eq. 9 is subject to the boundary conditions at the edges of the domain $0 \leq z \leq L$:

$$(10) \quad C(z = 0) = C_0$$

$$(11) \quad -D \times \frac{dC}{dz}(z = L) = J_{\text{fix}}$$

C_0 represents the initial concentration of $\text{CO}_{2(aq)}$, and J_{fix} ($=C_{\text{fix}}/[\text{SA} \times f_{\text{SA}}]$; Table S2) represents the carbon fixation rate normalized to the fraction (f_{SA}) of the surface area (SA) of the cell available to CO_2 transport. The final solution for C as a function of distance has the form:

$$(12) \quad C(z) = C_0 - \frac{J_{\text{fix}}}{D} \times z$$

In this expression, C_0 is in units of $\mu\text{g } \mu\text{m}^{-3}$, D is in units of $\mu\text{m}^2 \text{ s}^{-1}$, z is in units of μm and J_{fix} , is in units of $\mu\text{g C } \mu\text{m}^{-2} \text{ s}^{-1}$. The per-cell carbon fixation rates reflected in J_{fix} are calculated by dividing the measured carbon fixation rates in $\mu\text{g C cell}^{-1} \text{ s}^{-1}$ by the surface area of a cell, which we define as a rod with a radius of 0.5 μm and a length of 2 μm , as well as the fraction of the surface area of the cell available to CO_2 transport. (Table S2).

Similar equations apply for the heavy isotope (^{13}C):

$$(13) \quad {}^{13}\text{D} \times \frac{d^2}{dz^2} ({}^{13}\text{C}) = 0$$

Eq. 13 is subject to the boundary conditions at the edges of the domain $0 \leq z \leq L$:

$$(14) \quad {}^{13}\text{C}(z = 0) = {}^{13}\text{C}_0$$

$$(15) \quad -{}^{13}\text{D} \times \frac{d^{13}\text{C}}{dz}(z = L) = {}^{13}\text{J}_{\text{fix}}$$

The final solution for ${}^{13}\text{C}$ as a function of distance has the form:

$$(16) \quad {}^{13}\text{C}(z) = {}^{13}\text{A} + {}^{13}\text{B} \times z$$

${}^{13}\text{A}$ and ${}^{13}\text{B}$ are integration constants defined by the boundary conditions such that

$$(17) \quad {}^{13}\text{A} = {}^{13}\text{C}_0$$

$$(18) \quad -{}^{13}\text{D} \times {}^{13}\text{B} = {}^{13}\text{J}_{\text{fix}}.$$

We defined $^{13}J_{fix}$ through:

$$(19) \quad \alpha_{fix} = \frac{^{13}J_{fix}}{^{12}J_{fix}} / \frac{^{13}C_L}{^{12}C_L}$$

Here α_{fix} is the fractionation factor associated with CO₂ fixation by rubisco (Table S2), while $^{13}C_L$ and $^{12}C_L$ represent the concentrations of each isotopologue of CO₂ at z = L. Applying the trace isotope abundance approximation ($C_L \approx ^{12}C_L$, $J_{fix} \approx ^{12}J_{fix}$) leads to:

$$(20) \quad ^{13}J_{fix} = \alpha_{fix} \times J_{fix} \times \frac{^{13}C_L}{C_L}.$$

We combined Eqs. 18 and 20

$$(21) \quad -^{13}D \times ^{13}B = \alpha_{fix} \times J_{fix} \times \frac{^{13}C_L}{C_L}$$

to solve for ^{13}B :

$$(22) \quad ^{13}B = - \frac{\alpha_{fix} \frac{J_{fix}}{D} ^{13}C_0}{\alpha_{diff} C_L + \alpha_{fix} \frac{J_{fix}}{D} L}$$

Here α_{diff} is the fractionation factor associated with CO₂ diffusion to the site of fixation, which is defined as $\alpha_{diff} = ^{13}D / ^{12}D$ (Table S2). The final solution for ^{13}C is then:

$$(23) \quad ^{13}C(z) = ^{13}C_0 \left(1 - \frac{\alpha_{fix} \frac{J_{fix}}{D}}{\alpha_{diff} C_L + \alpha_{fix} \frac{J_{fix}}{D} L} z \right).$$

We then calculated ε_P as the difference between the carbon isotopic composition of fixed carbon and dissolved CO₂ using:

$$(24) \quad \varepsilon_P = \frac{\left(\frac{^{13}C_0}{^{12}C_0} - \alpha_{fix} \frac{^{13}C_L}{^{12}C_L} \right)}{\frac{^{13}C_0}{^{12}C_0}} \times 1000.$$

Independent model inputs are: the carbon fixation rates observed for the Δccm mutant grown under 1% and 3% CO₂ headspace, the concentration of dissolved CO₂ calculated from pCO_2 and the culture pH using the csys program (72), and the fractionation factor for diffusion of CO₂ in water ($\varepsilon_{diff} = [\alpha_{diff} - 1] \times 1000$; Table S2). Two previously published values of the fractionation factor for form IB

rubisco ($\varepsilon_{fix} = [\alpha_{fix} - 1] \times 1000$) in cyanobacteria are $22 \pm 0.2\%$ (74) and $20.9 \pm 0.8\%$ (75), both measured on rubisco from in *Synechococcus* PCC 6301. Here, we set ε_{fix} at 24.3% , the maximum whole-cell ε_P value we observed for *Synechococcus* 7002.

The model has three free physiological parameters: i) the intracellular distance over which $\text{CO}_{2(\text{aq})}$ diffuses (z); ii) the intracellular diffusion coefficient for $\text{CO}_{2(\text{aq})}$ (D); and iii) the proportion of cellular surface area available for diffusion (f_{SA}). Free parameters covary over the constrained ranges in Table S2. We trained the model by selecting the interdependent parameter sets that were able to reproduce experimental ε_P values observed in the *Synechococcus* 7002 Δccm mutant (within the $\approx 0.65\%$ data spread for a given experimental condition) at carbon fixation rates observed for both 1% and 3% headspace CO_2 (36 and 107 PAL, respectively). We then continued calculations and model predictions incorporating all interdependent parameter sets [z , D , f_{SA}] that could reproduce experimental ε_P values.

In order to apply the 1D reaction-diffusion model across varying CO_2 levels, we incorporated a previously published model of carbon fixation rate (76):

$$(25) \quad C_{fix} = \frac{k_{cat} N_{sites} C}{C + K_{m,CO_2} \left(1 + \frac{O}{K_{m,O_2}} \right)}$$

Here, C_{fix} represents the carbon fixation rate as a function of CO_2 (C) and O_2 (O) concentrations and rubisco kinetic parameters (values listed in Table S2). We fit this theoretical relationship through the observed range of carbon fixation rates using the kinetic parameters for Form IB rubisco in *Synechococcus* 7002 and number of rubisco sites per cell as $N_{sites} = 2.3 \times 10^5 - 3.4 \times 10^5$ (Fig. S8). However, this fit could be similarly achieved by scaling the rubisco kinetics to account for differences between calculated and measured carbon fixation rates. The trained dependence of carbon fixation rate on CO_2 concentration is then used as a model input to predict ε_P values at varying CO_2 and O_2 levels (Fig 2B). Modeled ε_P values increase with CO_2 concentration (Fig. S8). Values of ε_P show a greater dependence on carbon fixation at low CO_2 concentrations (Fig. S8B).

The trained model and corresponding carbon fixation rate calculation can then be used to predict ε_P values for a cyanobacterium without a carboxysome grown under varying CO_2 and O_2 conditions with independently derived kinetic parameters for rubisco (see next section).

7. Evolutionary changes in rubisco kinetics

The Δccm model exercise suggests that, without a CCM, fractionation by extant cyanobacteria with Form IB rubisco can only explain a limited portion of estimated middle Proterozoic ε_P values. The Δccm

model incorporates the kinetics and fractionation for modern Form 1B rubisco (Table S2). Here, we explore how evolutionary changes in rubisco kinetics could impact these modeling results.

Ancestral sequence reconstruction of Form IA and Form IB rubisco suggest that the kinetics of ancestral Form I rubiscos differed from modern rubisco, although the timing of these evolutionary changes remain unconstrained (42). For example, k_{cat} and K_{m, CO_2} values for ancestral rubiscos are ~40-80% of modern forms (42). While fractionation factors for these reconstructed rubisco (ε_{fix}) forms have not yet been characterized, the kinetics constrain how far ε_P values can deviate from a maximum ε_{fix} value and thus constrain the overall range of ε_P values accessible for a given ε_{fix} value. Substituting the kinetics associated with ancestral Form 1A and Form 1B rubisco, while keeping the rest of the model inputs constant, results in a 7-8‰ range in ε_P values for any given value of ε_{fix} for rubisco (Fig. S9). This range is less than half the 95th percentile range (~16‰) from our resampling of the mid-Proterozoic carbon isotope record suggesting that, regardless of the ancestral rubisco ε_{fix} value, net carbon isotope fractionation by cyanobacteria with these ancestral rubisco forms could not be responsible for the entire range of mid-Proterozoic ε_P estimates.

We additionally used the measured characteristics of different extant rubisco forms to determine the possible constraints imposed on ε_P by the relationship between kinetics and fractionation factors in cyanobacteria without a CCM. Model sensitivity runs based on paired inputs of rubisco kinetics compiled in (51) and fractionation factors compiled in (77) show the ε_P ranges accessed by Form 1A, Form 1B, and Form II rubiscos in cyanobacteria without a CCM (Fig. S9, Table S3). Similar to the results with the Δ_{CCM} mutant reported here, Form 1B rubiscos in extant cyanobacteria without a CCM can only reproduce a limited range of mid-Proterozoic ε_P values (Fig. S9). If Form II rubisco operated in cyanobacteria without a CCM it would be consistent with a similar range of estimates, while Form 1A rubisco would produce a much smaller range of ε_P values (Fig. S9). Only the kinetics and fractionation factors of Form 1B rubisco from higher plants (*Spinacia oleracea* and *Nicotiana tabacum*) produce ε_P ranges larger than the middle Proterozoic estimates, if they operated in cyanobacteria without a CCM (Fig. S9).

Form 1B rubiscos within extant higher green plants, such as the rubiscos found in *Spinacia oleracea* and *Nicotiana tabacum*, have kinetic parameters and $\varepsilon_{rubisco}$ values that yield substantially larger ranges of ε_P values when incorporated in the 1-D reaction-diffusion model developed for the Δ_{CCM} mutant of *Synechococcus* sp. 7002. This suggests that, if middle Proterozoic cyanobacteria contained rubiscos resembling Form 1B in higher green plants, a CCM would not be required to produce the full distribution of middle Proterozoic ε_P values. Archaeplastida are extant representatives of a primary endosymbiotic event, in which an original plastid, derived from an ancestral cyanobacterium, was incorporated into a eukaryotic host cell at ~1.3 Ga (21). Although it is possible that the kinetics of Form 1B rubiscos from Archaeplastida are a vestigial remnant of this ancient endosymbiotic event, it seems unlikely that the

selective environment provided by the early Proterozoic surface ocean was similar enough to that within green plant chloroplasts to maintain enzymatic stasis over the ensuing billion years. Altogether, this consideration of potential ancestral rubisco kinetics suggests that carbon isotope fractionation by cyanobacteria lacking a CCM is inconsistent with the estimated distribution of Proterozoic ε_P values.

Supplementary Figures and Tables

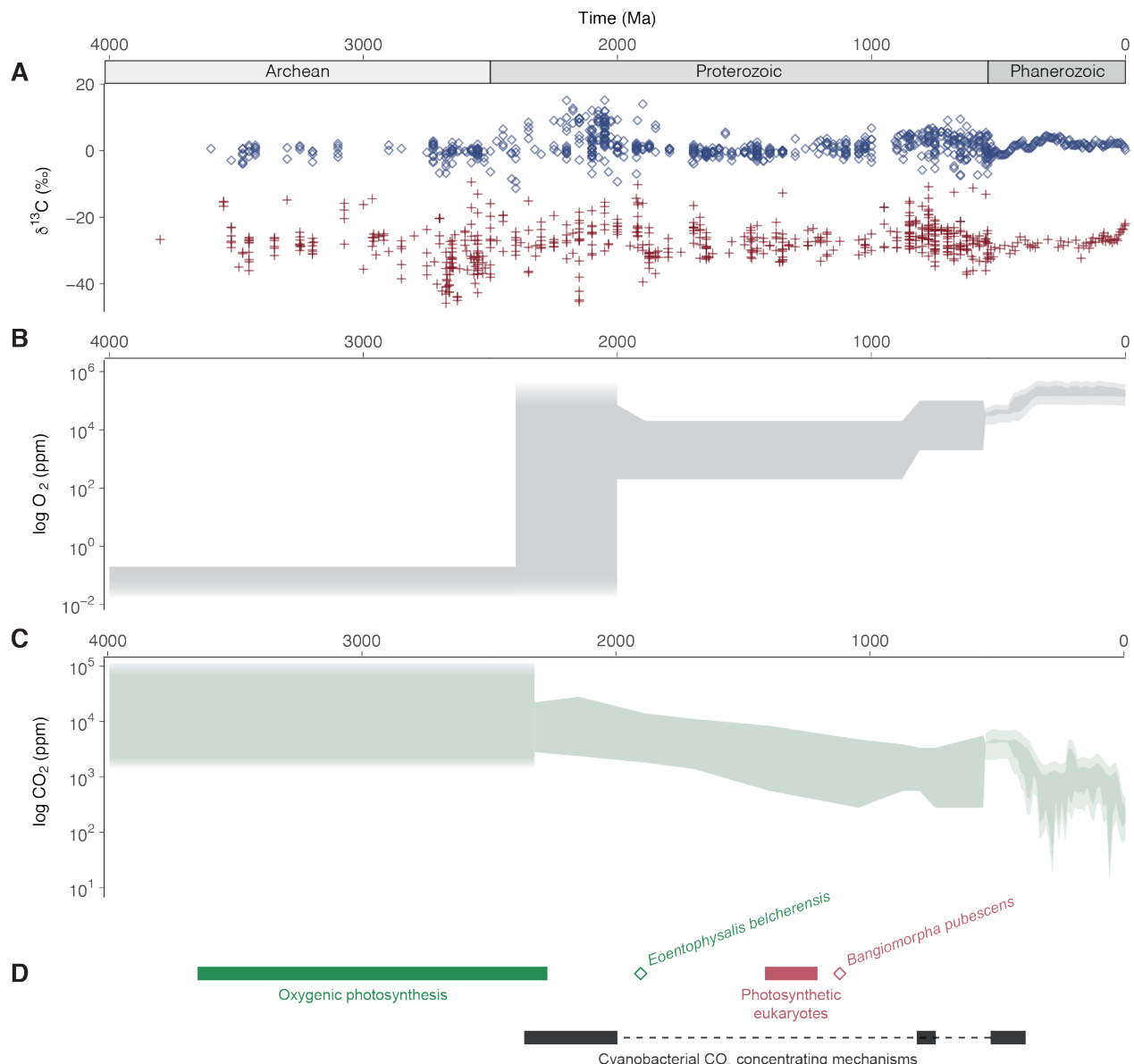


Fig. S1. The carbon isotope record and estimated atmospheric and biologic changes through Earth history. **A.** Values of $\delta^{13}\text{C}$ from carbonate minerals (blue) and $\delta^{13}\text{C}$ values of total organic carbon (red) are compiled in Krissansen-Totton et al., (24). **B.** Archean O_2 estimates restrict pO_2 to $< 10^{-6}$ present atmospheric levels or 2 ppm (4). Proterozoic O_2 estimates are compiled in Crockford et al., (8). Phanerozoic O_2 estimates come from proxies and modeling (59). **C.** Archean CO_2 estimates are from Halevy and Bachan (39). Proterozoic CO_2 estimates are compiled in Crockford et al., (8). Phanerozoic CO_2 estimates come from proxies and modeling (59). **D.** Range of estimates for the origin of oxygenic photosynthesis shown as a green bar (2, 3) and the earliest unambiguous cyanobacterial microfossils (*Eoentophysalis belcherensis*) shown as a green diamond (13, 14). Earliest unambiguous fossil photosynthetic eukaryote (*Bangiomorpha pubescens*) shown as a red diamond with corresponding molecular clock estimates for the primary plastid endosymbiosis shown as a red bar (21). Proposed dates for the emergence of a cyanobacterial CO_2 Concentrating Mechanism shown as black bars (e.g., 34).

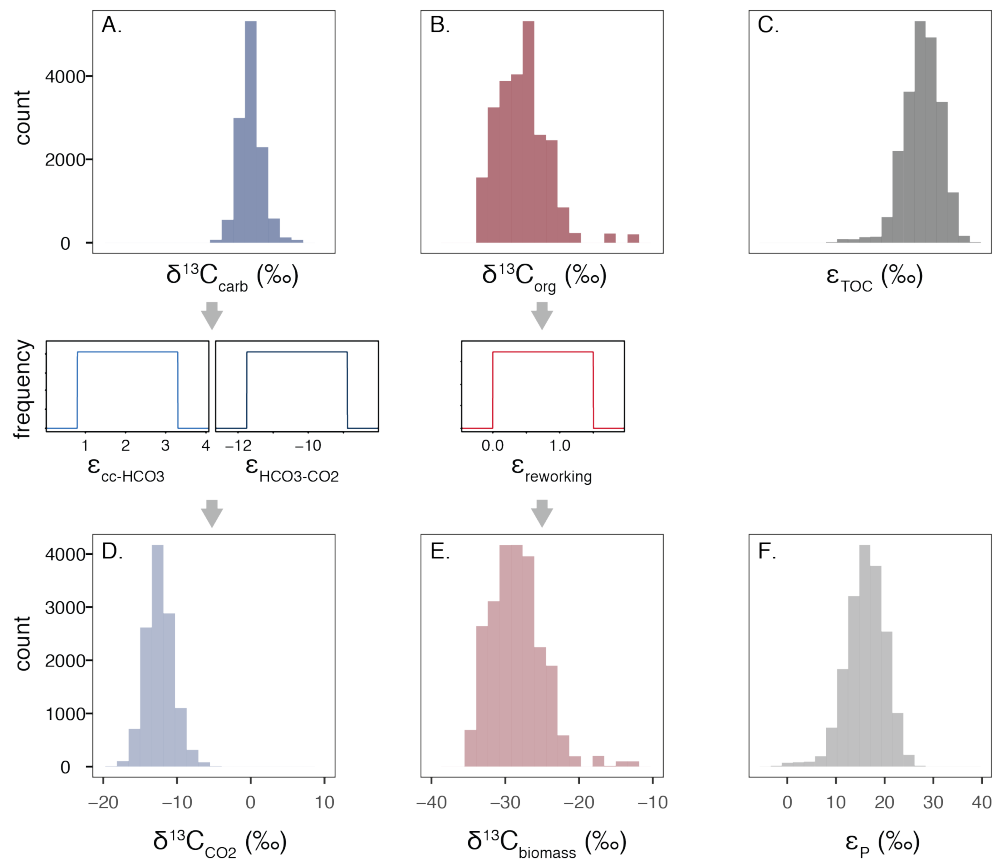


Fig. S2. Representation of bootstrap resampling and Monte Carlo simulations. **A.** Resampled $\delta^{13}\text{C}$ values of carbonates and **B.** organic carbon during the non-transitional period between 1.0-1.8 Ga from Krissansen-Totton et al. (24). **C.** The distribution of ε_{TOC} values from the bootstrap resampling, calculated according to Eq. 1. **D.** The distribution of predicted $\delta^{13}\text{C}$ values of dissolved CO_2 , calculated by incorporating the isotope effects associated with precipitation of calcite or aragonite from HCO_3^- and the conversion between HCO_3^- and dissolved CO_2 (inset uniform distributions $\varepsilon_{\text{cc-HCO}_3}$ and $\varepsilon_{\text{HCO}_3-\text{CO}_2}$). **E.** The distribution of predicted $\delta^{13}\text{C}$ values of primary biomass calculated by incorporating an isotope effect associated with secondary reworking in the water column and sediments (inset uniform distribution $\varepsilon_{\text{reworking}}$). **F.** The distribution of predicted ε_{P} values calculated according to Eq. 2. See text for simulation details.

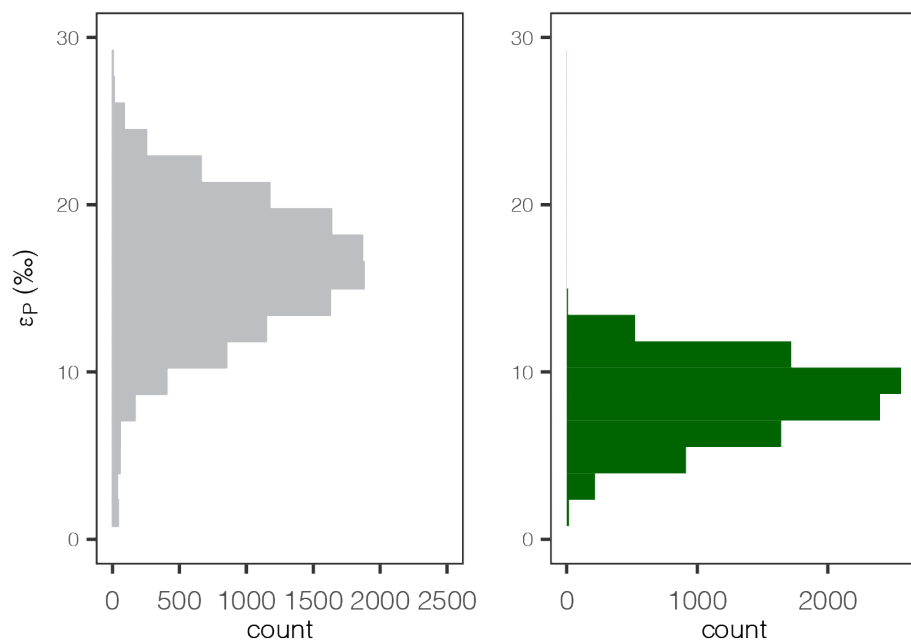


Fig. S3. Comparing the ϵ_P distribution between the middle Proterozoic (left) and a modern cyanobacterial mat (right). Both distributions are the result of Monte Carlo simulations and bootstrap resampling of sedimentary carbon isotope records (left) and a previously published isotopic characterization of a cyanobacterial mat (right; 26).

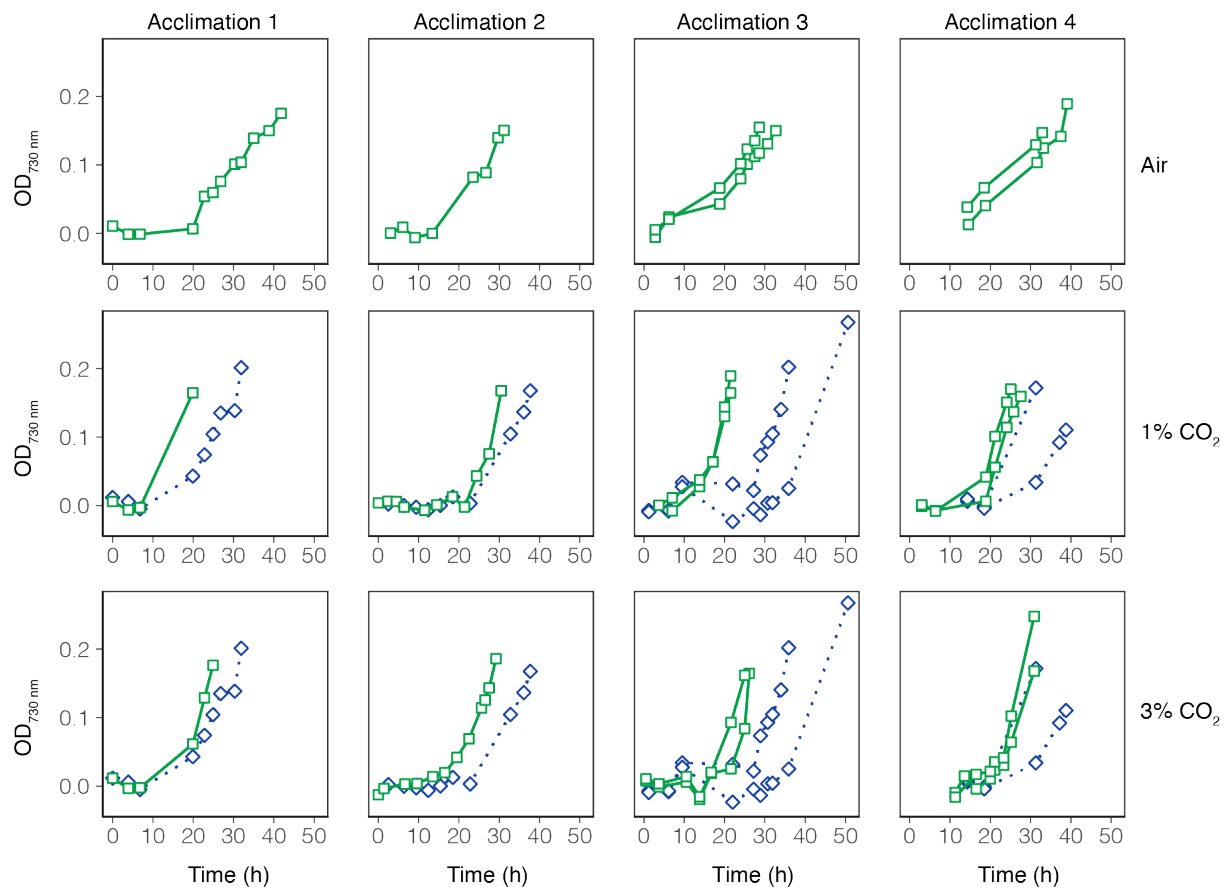


Fig. S4. Growth curves for cultures of *Synechococcus* 7002 in air, 1% CO₂, and 3% CO₂ corresponding to 1, 36, and 107 PAL CO₂. Green squares and solid lines represent wild-type *Synechococcus* 7002. Blue diamonds and dashed lines represent the Δccm mutant.

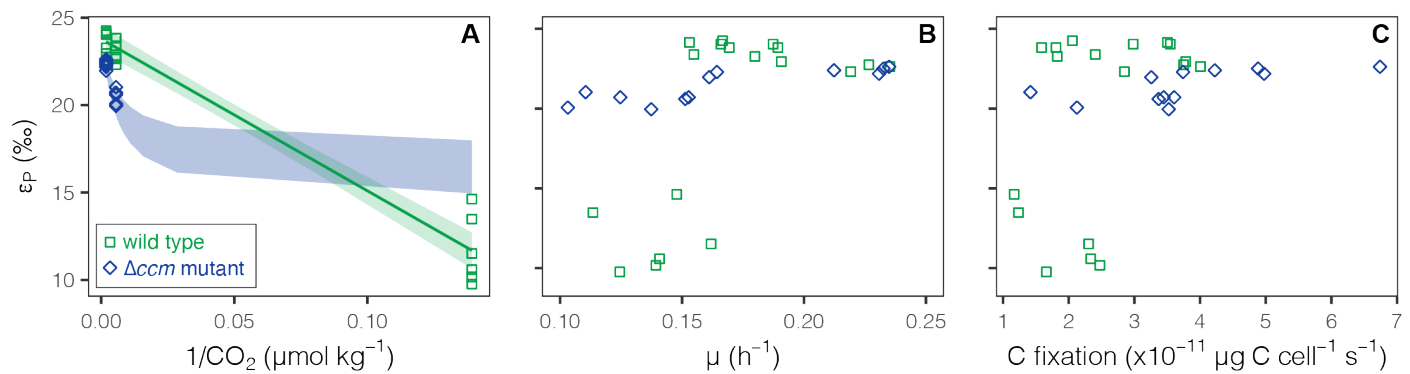


Fig. S5. The dependence of ε_P values observed in *Synechococcus* 7002 cultures on CO_2 and growth parameters. **A.** Values of ε_P in the wild-type strain (green symbols) show a linear dependence on $1/\text{CO}_2$ (green line; $R^2: 0.96$, shading represents 95% confidence interval). Values of ε_P in the Δccm strain (blue symbols) were used to model the dependence of ε_P on CO_2 concentration (blue shading). **B.** Values of ε_P do not vary systematically with specific growth rate (μ). **C.** The relationship between carbon fixation rate and ε_P values used to train the Δccm strain model.

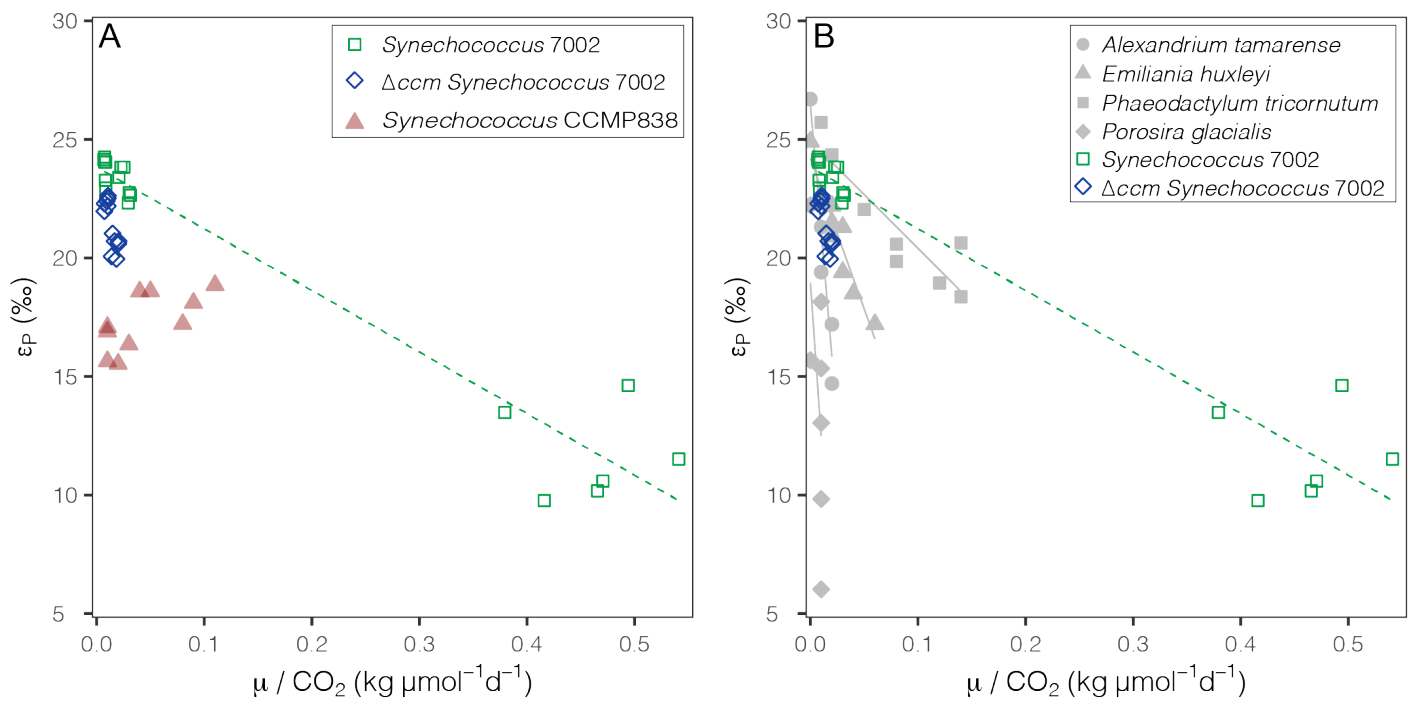


Fig. S6. Cyanobacterial and algal ϵ_P relationships. **A.** Cyanobacterial ϵ_P relationships observed in wild-type *Synechococcus* 7002 and Δccm mutant (this study) differ from the ϵ_P relationship found in alpha cyanobacterium *Synechococcus* CCMP838 (28). **B.** ϵ_P relationships found in wild type *Synechococcus* 7002 and Δccm mutant resemble ϵ_P relationships in eukaryotic algae (78).

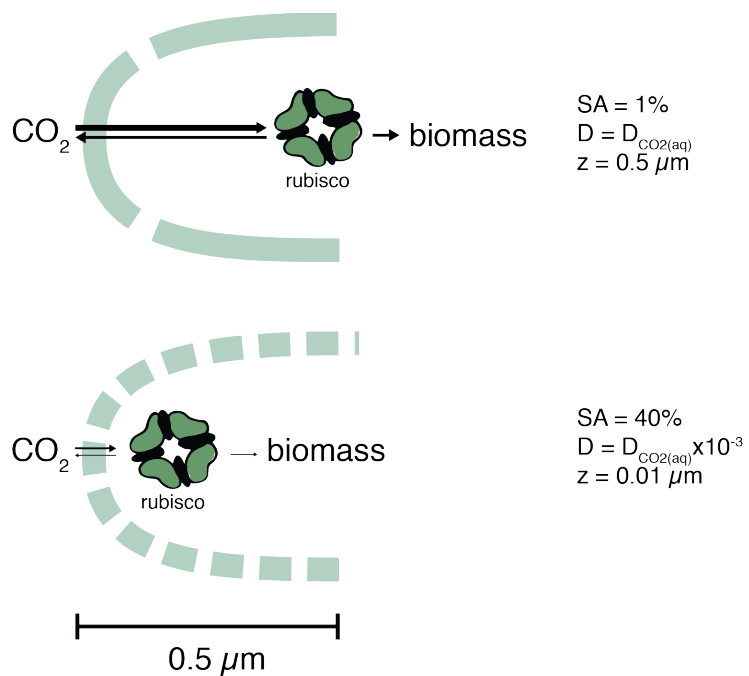


Fig. S7. 1D reaction-diffusion model. Fluxes include diffusion of CO₂ into the cell, autotrophic carbon fixation through the Calvin-Benson cycle, and diffusion of CO₂ out of the cell. The three interdependent model parameters are the surface area available for diffusion of CO₂ (SA), the diffusion coefficient for CO₂ at 37°C (D), and the distance to the rubisco active site (z). Example values of these parameters are shown here to illustrate the range of values possible for each parameter.

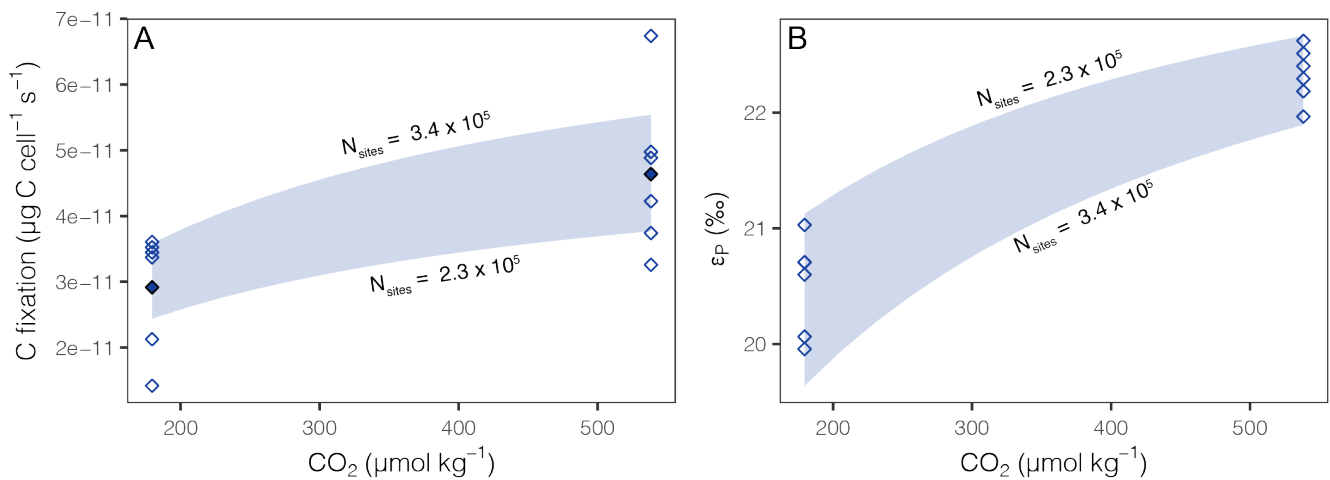


Fig. S8. Carbon fixation rate and ε_P values as a function of dissolved CO_2 concentration in the Δccm mutant. **A:** Open symbols represent measured carbon fixation rate for cultures of the Δccm mutant grown under a 1% and 3% CO_2 headspace (36 and 107 PAL CO_2). The shaded area represents the theoretical relationship between carbon fixation rate and CO_2 concentration from Clark et al. (76) fit to the observed culture data using the number of rubisco sites (N_{sites}). This fit could be similarly achieved by scaling the rubisco kinetics or incorporating an unknown factor to account for differences between the theoretical model and the measured carbon fixation rates. **B:** The carbon fixation rate as a function of dissolved CO_2 concentration is then used as a model input to predict corresponding ε_P values.

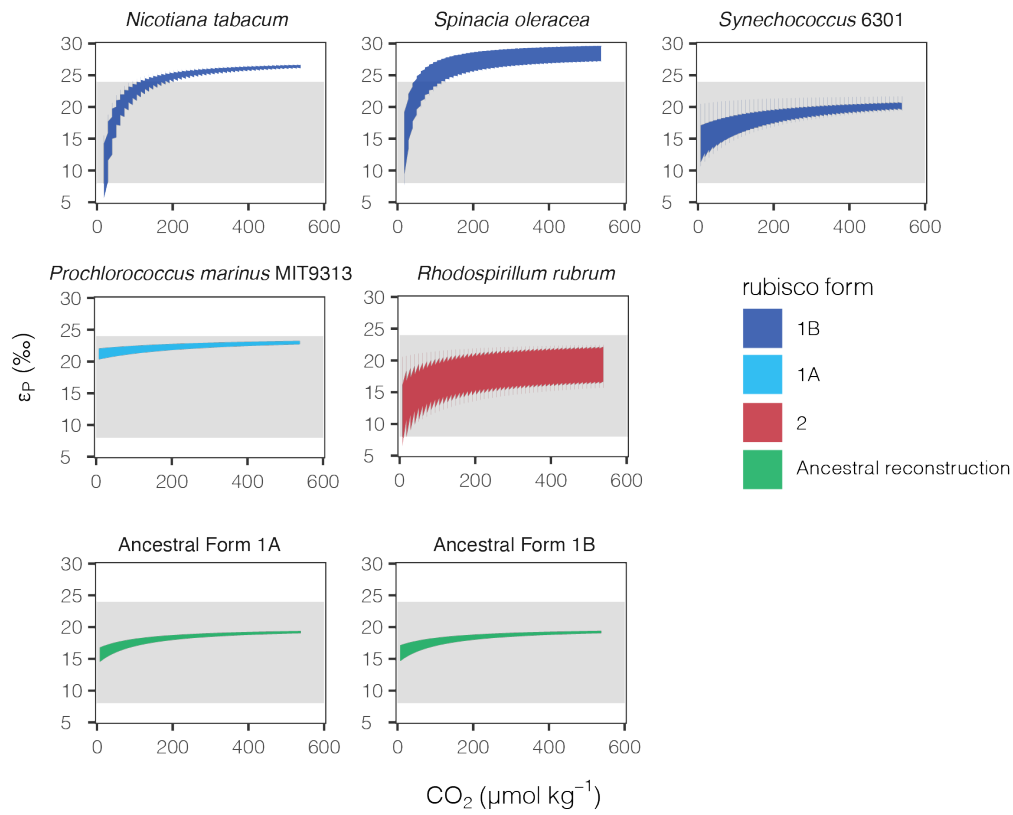


Fig. S9. The modeled relationship between ε_P values and CO_2 for both extant rubisco and ancestral reconstructions. The grey band represents the estimated middle Proterozoic distribution of ε_P (95th percentile; 8-24%). For extant rubisco forms, colored fields represent model results with ε_{fix} values from (77) and rubisco kinetics from (51) listed in Table S3. For the ancestral forms, colored fields represent model results with an example ε_{fix} value of 20‰ and kinetic parameters from (42). In all cases the model was run over O_2 concentrations of 0.14-14 $\mu\text{mol l}^{-1}$ (0.1-10% PAL).

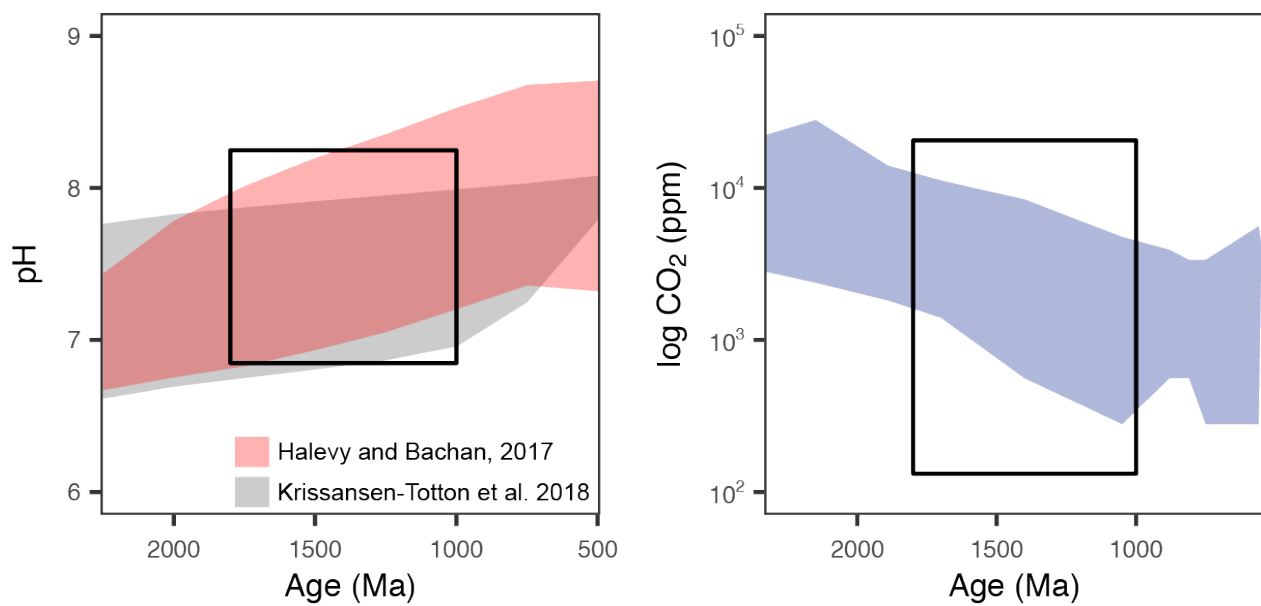


Fig. S10. Experimental culture conditions projected onto Proterozoic $p\text{CO}_2$ and pH estimates. The height of the boxes represents the experimental range of pH (left) and dissolved CO_2 translated into $p\text{CO}_2$ levels using the culture pH between assumed Proterozoic ocean temperatures of 3-30°C (right). The width of the box represents the middle Proterozoic time period resampled for the statistical simulations of the carbon isotope record. Estimates of Proterozoic pH are 95% confidence intervals from (39) and (38). Estimates of Proterozoic $p\text{CO}_2$ levels are from (8).

Supplementary Table 1. Growth parameters for wild type *Synechococcus* 7002 and Δccm mutant. Net specific growth rate was calculated according to Eq. S6. Carbon fixation rates (C_{fix}) was calculated according to Eq. S7. Analytical error for $\delta^{13}\text{C}_{\text{biomass}}$ values is $\pm 0.1\text{\textperthousand}$ and $0.01\text{\textperthousand}$ for $\delta^{13}\text{C}_{\text{CO}_2}$ values. Values of $\delta^{13}\text{C}_{\text{CO}_2}$ in air are from <https://www.esrl.noaa.gov/gmd/dv/iadv/index.php> (Niwot Ridge site).

Headspace CO_2 (PAL)	CO_2 ($\mu\text{mol kg}^{-1}$)	Strain	Acclimation	Doubling time (h)	C_{fix} (fg C cell $^{-1}$ h $^{-1}$)	$\delta^{13}\text{C}_{\text{biomass}}$ (\textperthousand)	$\delta^{13}\text{C}_{\text{CO}_2}$ (\textperthousand)	ϵ_P (\textperthousand)
1	7	WT	1	6.1	44	-22.5	-8.0	13.5 \pm 0.1
1	7	WT	2	4.7	42	-23.5	-8.0	14.6 \pm 0.1
1	7	WT	3	4.9	84	-19.6	-8.0	10.6 \pm 0.1
1	7	WT	3	4.3	83	-20.4	-8.0	11.5 \pm 0.1
1	7	WT	4	5.6	60	-18.7	-8.0	9.8 \pm 0.1
1	7	WT	4	5.0	89	-19.1	-8.0	10.2 \pm 0.1
36	180	WT	1	3.0	144	-50.2	-27.7	22.6 \pm 0.1
36	180	WT	2	4.5	87	-50.8	-27.7	23.4 \pm 0.1
36	180	WT	3	3.1	135	-50.1	-27.7	22.7 \pm 0.1
36	180	WT	3	3.2	103	-49.8	-27.7	22.3 \pm 0.1
36	180	WT	4	4.1	65	-51.1	-27.7	23.8 \pm 0.1
36	180	WT	4	3.7	57	-51.1	-27.7	23.8 \pm 0.1
107	538	WT	1	3.6	136	-63.0	-40.6	22.9 \pm 0.1
107	538	WT	2	4.2	107	-63.9	-40.6	24.0 \pm 0.1
107	538	WT	3	3.9	66	-63.1	-40.6	23.3 \pm 0.1
107	538	WT	3	3.7	128	-63.8	-40.6	24.0 \pm 0.1
107	538	WT	4	4.5	126	-63.8	-40.6	24.1 \pm 0.1
107	538	WT	4	4.2	74	-63.9	-40.6	24.3 \pm 0.1
36	180	Δccm	1	4.5	130	-48.3	-27.7	20.7 \pm 0.1
36	180	Δccm	2	5.6	124	-48.3	-27.7	20.7 \pm 0.1
36	180	Δccm	3	5.1	127	-47.5	-27.7	20.0 \pm 0.1
36	180	Δccm	3	6.7	77	-47.7	-27.7	20.1 \pm 0.1
36	180	Δccm	4	4.6	121	-48.0	-27.7	20.6 \pm 0.1
36	180	Δccm	4	6.3	51	-48.4	-27.7	21.0 \pm 0.1
107	538	Δccm	1	4.2	135	-62.4	-40.6	22.3 \pm 0.1
107	538	Δccm	2	4.3	117	-61.9	-40.6	22.0 \pm 0.1
107	538	Δccm	3	3.3	152	-62.2	-40.6	22.4 \pm 0.1
107	538	Δccm	3	3.0	179	-62.1	-40.6	22.2 \pm 0.1
107	538	Δccm	4	3.0	176	-62.3	-40.6	22.5 \pm 0.1
107	538	Δccm	4	3.0	243	-62.3	-40.6	22.6 \pm 0.1

Supplementary Table 2. 1D reaction-diffusion model parameters.

Parameter	Description	Values	Units	Notes
C_{fix}	Measured C fixation rate	1.4×10^{-11} - 6.7×10^{-11}	$\mu\text{g C cell}^{-1} \text{s}^{-1}$	Grown under 25-75 PAL CO ₂
J_{fix}	Converted C fixation rate		$\mu\text{g C } \mu\text{m}^{-2} \text{s}^{-1}$	$C_{fix}/(\text{SA} \times f\text{SA})$
C_0	Experimental dissolved [CO ₂]	8.8×10^{-14} - 6.6×10^{-12}	$\mu\text{g C } \mu\text{m}^{-3}$	Calculated from <i>p</i> CO ₂ and pH using csys (72)
z	Distance to the sink	0.01-0.5	μm	Based on a cell with a radius of 0.5 μm
SA	Surface area of a rod	6.3	μm^2	Based on a rod with a radius of 0.5 μm and a length of 2 μm representing a cyanobacterial cell
fSA	Effective surface area	0.01-0.4	fraction	Proportion of surface area available for diffusion of CO ₂
D	Diffusion coefficient CO ₂	26.9-2690	$\mu\text{m}^2 \text{s}^{-1}$	Constrained by the diffusion coefficient of CO _{2(aq)} in water ($2.69 \times 10^3 \mu\text{m}^2 \text{s}^{-1}$ at 37°C) (79)
α_{diff}	Fractionation associated with diffusion of CO ₂	1.00087		O'Leary et al. (80)
α_{fix}	Fractionation associated with rubisco	1.0243		Note 1.
k_{cat}	form IB rubisco	11.4	molecules site ⁻¹ s ⁻¹	adapted from Clark et al. (76)
K_{m, CO_2}	form IB rubisco	185	$\mu\text{mol l}^{-1}$	adapted from Clark et al. (76)
K_{m, O_2}	form IB rubisco	1300	$\mu\text{mol l}^{-1}$	adapted from Clark et al. (76)
O_2	Concentration of dissolved O ₂	143	$\mu\text{mol l}^{-1}$	Calculated. Note 2.
Nsites	rubisco active sites	2.3×10^5 - 3.4×10^5	number	Note 3.

¹ Previously published fractionation for form IB rubisco in *Synechococcus* PCC 6301 are $22 \pm 0.2\%$ (74)

and 20.9 ± 0.8 (75). Here, we set ε_{fix} at 24.3%, the maximum whole-cell ε_P value we observed for *Synechococcus* 7002.

² The concentration of dissolved oxygen was calculated from DOTABLES from the USGS (<https://www.usgs.gov/software/dotables>) using growth medium conditions of 37°C, 0.821 atm, and 32% salinity.

³ The number of rubisco active sites was used to fit the theoretical relationship (76) through the observed range of carbon fixation rates at 36 and 107 PAL. This fit could be similarly achieved by scaling the rubisco kinetics.

Supplementary Table 3. Model inputs for rubisco characteristics from extant organisms and ancestral state reconstructions (ASR). Values for ε_{fix} from (77), kinetic parameters for extant rubiscos from (51), kinetic parameters for ancestral rubiscos from (42)

Source	Form	ε_{fix}	$k_{\text{cat}} (\text{s}^{-1})$			$K_m \text{CO}_2 (\mu\text{M})$			$K_m \text{O}_2 (\mu\text{M})$			Taxonomy
ASR	Anc. 1B	--	4.77	\pm	0.1	113	\pm	6	2010	\pm	571	Ancestral
ASR	Anc. 1A	--	4.72	\pm	0.1	120	\pm	10	641	\pm	49	Ancestral
Spinacia oleracea	1B	29.3	2.9	\pm	0.2	10	\pm	1	250	\pm	33	C3 plants
Spinacia oleracea	1B	29.3	3.2	\pm	0.1	12.1	\pm	1	574	\pm	19	C3 plants
Spinacia oleracea	1B	29.3	3.2	\pm	0.1	12.1	\pm	1	574	\pm	19	C3 plants
Spinacia oleracea	1B	29.3	2.7	\pm	0.1	11	\pm	2	520	\pm	25	C3 plants
Nicotiana tabacum	1B	27.4	3.9	\pm	0.2	9	\pm	0	292	\pm	20	C3 plants
Nicotiana tabacum	1B	27.4	3.4	\pm	0.1	10.7	\pm	1	295	\pm	71	C3 plants
Nicotiana tabacum	1B	27.4	3.1	\pm	0.3	9.7	\pm	0	283	\pm	15	C3 plants
Nicotiana tabacum	1B	27.4	3.4	\pm	0.1	10.7	\pm	1	295	\pm	71	C3 plants
Synechococcus 6301	1B	22.0	11.4	\pm	0.7	185	\pm	17	1300	\pm	172	Cyanobacteria
Synechococcus 6301	1B	22.0	12	\pm	0.7	167	\pm	15	529	\pm	69.8	Cyanobacteria
Synechococcus 6301	1B	22.0	11.8	\pm	0.2	200	\pm	9	199	\pm	42	Cyanobacteria
Synechococcus 6301	1B	22.0	2.57	\pm	0.2	142	\pm	1	664	\pm	82	Cyanobacteria
Synechococcus 6301	1B	22.0	3.71	\pm	0.2	167	\pm	2	529	\pm	14	Cyanobacteria
Synechococcus 6301	1B	22.0	11.6	\pm	0.4	340	\pm	12	972	\pm	26	Cyanobacteria
Synechococcus 6301	1B	22.0	9.78	\pm	0.5	152	\pm	23	1230	\pm	135	Cyanobacteria
Prochlorococcus marinus MIT9313	1A	24.0	6.58	\pm	0.3	309	\pm	24	1400	\pm	300	Cyanobacteria
Rhodospirillum rubrum	2	20.4	5.7	\pm	0.3	89	\pm	8	406	\pm	53.6	Alphaproteobacteria
Rhodospirillum rubrum	2	20.4	12.3	\pm	0.3	149	\pm	8	159	\pm	25	Alphaproteobacteria
Rhodospirillum rubrum	2	20.4	4.3	\pm	0.5	125	\pm	12	143	\pm	3	Alphaproteobacteria
Rhodospirillum rubrum	2	20.4	7.3	\pm	0.3	80	\pm	11	406	\pm	48	Alphaproteobacteria

REFERENCES AND NOTES

1. D. E. Canfield, The early history of atmospheric oxygen: Homage to Robert M. Garrels. *Annu. Rev. Earth Planet. Sci.* **33**, 1–36 (2005).
2. W. W. Fischer, J. Hemp, J. E. Johnson, Evolution of oxygenic photosynthesis. *Annu. Rev. Earth Planet. Sci.* **44**, 647–683 (2016).
3. P. Sánchez-Baracaldo, T. Cardona, On the origin of oxygenic photosynthesis and Cyanobacteria. *New Phytol.* **225**, 1440–1446 (2020).
4. D. C. Catling, K. J. Zahnle, The Archean atmosphere. *Sci. Adv.* **6**, eaax1420 (2020).
5. M. S. W. Hodgskiss, P. W. Crockford, Y. Peng, B. A. Wing, T. J. Horner, A productivity collapse to end Earth’s Great Oxidation. *Proc. Natl. Acad. Sci. U.S.A.* **116**, 17207–17212 (2019).
6. N. J. Planavsky, C. T. Reinhard, X. Wang, D. Thomson, P. McGoldrick, R. H. Rainbird, T. Johnson, W. W. Fischer, T. W. Lyons, Low mid-Proterozoic atmospheric oxygen levels and the delayed rise of animals. *Science* **346**, 635–638 (2014).
7. P. W. Crockford, J. A. Hayles, H. Bao, N. J. Planavsky, A. Bekker, P. W. Fralick, G. P. Halverson, T. H. Bui, Y. Peng, B. A. Wing, Triple oxygen isotope evidence for limited mid-Proterozoic primary productivity. *Nature* **559**, 613–616 (2018).
8. P. W. Crockford, M. Kunzmann, A. Bekker, J. Hayles, H. Bao, G. P. Halverson, Y. Peng, T. H. Bui, G. M. Cox, T. M. Gibson, S. Wörndle, R. Rainbird, A. Lepland, N. L. Swanson-Hysell, S. Master, B. Sreenivas, A. Kuznetsov, V. Krupenik, B. A. Wing, Claypool continued: Extending the isotopic record of sedimentary sulfate. *Chem. Geol.* **513**, 200–225 (2019).
9. M. A. Kipp, E. E. Stüeken, Biomass recycling and Earth’s early phosphorus cycle. *Sci. Adv.* **3**, eaao4795 (2017).
10. S. L. Olson, C. T. Reinhard, T. W. Lyons, Cyanobacterial diazotrophy and Earth’s delayed oxygenation. *Front. Microbiol.* **7**, 1526 (2016).
11. C. Scott, T. W. Lyons, A. Bekker, Y. Shen, S. W. Poulton, X. Chu, A. D. Anbar, Tracing the stepwise oxygenation of the Proterozoic ocean. *Nature* **452**, 456–459 (2008).
12. K. Ozaki, K. J. Thompson, R. L. Simister, S. A. Crowe, C. T. Reinhard, Anoxygenic photosynthesis and the delayed oxygenation of Earth’s atmosphere. *Nat. Commun.* **10**, 3026 (2019).
13. H. J. Hofmann, Precambrian Microflora, Belcher Islands, Canada: Significance and systematics. *J. Paleo.* **50**, 1040–1073 (1976).
14. M. S. W. Hodgskiss, O. M. J. Dagnaud, J. L. Frost, G. P. Halverson, M. D. Schmitz, N. L. Swanson-Hysell, E. A. Sperling, New insights on the Orosirian carbon cycle, early Cyanobacteria, and the

assembly of Laurentia from the Paleoproterozoic Belcher Group. *Earth Planet. Sci. Lett.* **520**, 141–152 (2019).

15. L. C. Kah, A. H. Knoll, Microbenthic distribution of Proterozoic tidal flats: Environmental and taphonomic considerations. *Geology* **24**, 79–82 (1996).
16. V. N. Sergeev, M. Sharma, Y. Shukla, Proterozoic fossil cyanobacteria. *Palaeobotanist* **61**, 189–358 (2012).
17. C. F. Demoulin, Y. J. Lara, L. Cornet, C. François, D. Baurain, A. Wilmotte, E. J. Javaux, Cyanobacteria evolution: Insight from the fossil record. *Free Radic. Biol. Med.* **140**, 206–223 (2019).
18. P. Sánchez-Baracaldo, Origin of marine planktonic cyanobacteria. *Sci. Rep.* **5**, 17418 (2015).
19. A. H. Knoll, R. E. Summons, J. R. Waldbauer, J. E. Zumberge, The geological succession of primary producers in the oceans, in *Evolution of Primary Producers in the Sea* (Elsevier, 2007), pp. 133–163.
20. N. Gueneli, A. M. McKenna, N. Ohkouchi, C. J. Boreham, J. Beghin, E. J. Javaux, J. J. Brocks, 1.1-billion-year-old porphyrins establish a marine ecosystem dominated by bacterial primary producers. *Proc. Natl. Acad. Sci. U.S.A.* **115**, E6978–E6986 (2018).
21. T. M. Gibson, P. M. Shih, V. M. Cumming, W. W. Fischer, P. W. Crockford, M. S. W. Hodgskiss, S. Wörndle, R. A. Creaser, R. H. Rainbird, T. M. Skulski, G. P. Halverson, Precise age of *Bangiomorpha pubescens* dates the origin of eukaryotic photosynthesis. *Geology* **46**, 135–138 (2017).
22. J. J. Brocks, A. J. M. Jarrett, E. Sirantoiné, C. Hallmann, Y. Hoshino, T. Liyanage, The rise of algae in Cryogenian oceans and the emergence of animals. *Nature* **548**, 578–581 (2017).
23. J. M. Hayes, H. Strauss, A. J. Kaufman, The abundance of ^{13}C in marine organic matter and isotopic fractionation in the global biogeochemical cycle of carbon during the past 800 Ma. *Chem. Geol.* **161**, 103–125 (1999).
24. J. Krissansen-Totton, R. Buick, D. C. Catling, A statistical analysis of the carbon isotope record from the Archean to Phanerozoic and implications for the rise of oxygen. *Am. J. Sci.* **315**, 275–316 (2015).
25. J. Schopf, M. Walter, in *The Biology of Cyanobacteria*, N.G. Carr, B.A. Whitton, eds. (Blackwell, 1982), pp. 543–564.
26. M. Schidlowski, H. Gorzawski, I. Dor, Carbon isotope variations in a solar pond microbial mat: Role of environmental gradients as steering variables. *Geochim. Cosmochim. Acta* **58**, 2289–2298 (1994).

27. D. J. Des Marais, D. E. Canfield, The carbon isotope biogeochemistry of microbial mats, in *Microbial Mats: Structure, Development and Environmental Significance*, L. J. Stal, P. Caumette, Eds. (Springer Berlin Heidelberg, 1994), pp. 289–298.

28. B. N. Popp, E. A. Laws, R. R. Bidigare, J. E. Dore, K. L. Hanson, S. G. Wakeham, Effect of phytoplankton cell geometry on carbon isotopic fractionation. *Geochim. Cosmochim. Acta* **62**, 69–77 (1998).

29. B. D. Rae, B. M. Long, M. R. Badger, G. D. Price, Functions, compositions, and evolution of the two types of carboxysomes: Polyhedral microcompartments that facilitate CO₂ fixation in cyanobacteria and some proteobacteria. *Microbiol. Mol. Biol. Rev.* **77**, 357–379 (2013).

30. T. D. Sharkey, Discovery of the canonical Calvin–Benson cycle. *Photosynth. Res.* **140**, 235–252 (2019).

31. J. C. Cameron, S. C. Wilson, S. L. Bernstein, C. A. Kerfeld, Biogenesis of a bacterial organelle: The carboxysome assembly pathway. *Cell* **155**, 1131–1140 (2013).

32. N. C. Hill, J. W. Tay, S. Altus, D. M. Bortz, J. C. Cameron, Life cycle of a cyanobacterial carboxysome. *Sci. Adv.* **6**, eaba1269 (2020).

33. P. Mahinthichaichan, D. M. Morris, Y. Wang, G. J. Jensen, E. Tajkhorshid, Selective permeability of carboxysome shell pores to anionic molecules. *J. Phys. Chem. B* **122**, 9110–9118 (2018).

34. M. Giordano, J. Beardall, J. A. Raven, CO₂ concentrating mechanisms in algae: Mechanisms, environmental modulation, and evolution. *Annu. Rev. Plant Biol.* **56**, 99–131 (2005).

35. L. Whitehead, B. M. Long, G. D. Price, M. R. Badger, Comparing the in vivo function of α -carboxysomes and β -carboxysomes in two model cyanobacteria. *Plant Physiol.* **165**, 398–411 (2014).

36. G. C. Gordon, T. C. Korosh, J. C. Cameron, A. L. Markley, M. B. Begemann, B. F. Pfleger, CRISPR interference as a titratable, *trans*-acting regulatory tool for metabolic engineering in the cyanobacterium *Synechococcus* sp. strain PCC 7002. *Metab. Eng.* **38**, 170–179 (2016).

37. R. L. Clark, G. C. Gordon, N. R. Bennett, H. Lyu, T. W. Root, B. F. Pfleger, High-CO₂ requirement as a mechanism for the containment of genetically modified cyanobacteria. *ACS Synth. Biol.* **7**, 384–391 (2018).

38. J. Krissansen-Totton, G. N. Arney, D. C. Catling, Constraining the climate and ocean pH of the early Earth with a geological carbon cycle model. *Proc. Natl. Acad. Sci.* **115**, 4105–4110 (2018).

39. I. Halevy, A. Bachan, The geologic history of seawater pH. *Science* **355**, 1069–1071 (2017).

40. E. A. Laws, B. N. Popp, R. R. Bidigare, M. C. Kennicutt, S. A. Macko, Dependence of phytoplankton carbon isotopic composition on growth rate and $[\text{CO}_2]_{\text{aq}}$: Theoretical considerations and experimental results. *Geochim. Cosmochim. Acta* **59**, 1131–1138 (1995).

41. B. Kacar, V. Hanson-Smith, Z. R. Adam, N. Boekelheide, Constraining the timing of the Great Oxidation Event within the Rubisco phylogenetic tree. *Geobiology* **15**, 628–640 (2017).

42. P. M. Shih, A. Occhialini, J. C. Cameron, P. J. Andralojc, M. A. J. Parry, C. A. Kerfeld, Biochemical characterization of predicted Precambrian RuBisCO. *Nat. Commun.* **7**, 10382 (2016).

43. M. Lebrato, D. Garbe-Schönberg, M. N. Müller, S. Blanco-Ameijeiras, R. A. Feely, L. Lorenzoni, J.-C. Molinero, K. Bremer, D. O. B. Jones, D. Iglesias-Rodriguez, D. Greeley, M. D. Lamare, A. Paulmier, M. Graco, J. Cartes, J. Barcelos e Ramos, A. de Lara, R. Sanchez-Leal, P. Jimenez, F. E. Paparazzo, S. E. Hartman, U. Westernströer, M. Küter, R. Benavides, A. F. da Silva, S. Bell, C. Payne, S. Olafsdottir, K. Robinson, L. M. Jantunen, A. Koralev, R. J. Webster, E. M. Jones, O. Gilg, P. B. du Bois, J. Beldowski, C. Ashjian, N. D. Yahia, B. Twining, X.-G. Chen, L.-C. Tseng, J.-S. Hwang, H.-U. Dahms, A. Oschlies, Global variability in seawater Mg:Ca and Sr:Ca ratios in the modern ocean. *Proc. Natl. Acad. Sci. U.S.A.* **117**, 22281–22292 (2020).

44. K.-H. Tang, Y. Tang, R. E. Blankenship, Carbon metabolic pathways in phototrophic bacteria and their broader evolutionary implications. *Front. Microbiol.* **2**, 165 (2011).

45. L. C. Kah, R. Riding, Mesoproterozoic carbon dioxide levels inferred from calcified cyanobacteria. *Geology* **35**, 799–802 (2007).

46. G. D. Price, M. R. Badger, F. J. Woodger, B. M. Long, Advances in understanding the cyanobacterial CO_2 -concentrating-mechanism (CCM): Functional components, Ci transporters, diversity, genetic regulation and prospects for engineering into plants. *J. Exp. Bot.* **59**, 1441–1461 (2008).

47. H. Bauwe, M. Hagemann, A. R. Fernie, Photorespiration: Players, partners and origin. *Trends Plant Sci.* **15**, 330–336 (2010).

48. A. Bachan, L. R. Kump, The rise of oxygen and siderite oxidation during the Lomagundi Event. *Proc. Natl. Acad. Sci. U.S.A.* **112**, 6562–6567 (2015).

49. S. Kihara, D. A. Hartzler, S. Savikhin, Oxygen concentration inside a functioning photosynthetic cell. *Biophys. J.* **106**, 1882–1889 (2014).

50. G. C. Cannon, C. E. Bradburne, H. C. Aldrich, S. H. Baker, S. Heinhorst, J. M. Shively, Microcompartments in prokaryotes: Carboxysomes and related polyhedra. *Appl. Environ. Microbiol.* **67**, 5351–5361 (2001).

51. A. I. Flamholz, N. Prywes, U. Moran, D. Davidi, Y. M. Bar-On, L. M. Oltrogge, R. Alves, D. Savage, R. Milo, Revisiting trade-offs between Rubisco kinetic parameters. *Biochemistry* **58**, 3365–3376 (2019).
52. J. W. Schopf, Disparate rates, differing fates: Tempo and mode of evolution changed from the Precambrian to the Phanerozoic. *Proc. Natl. Acad. Sci. U.S.A.* **91**, 6735–6742 (1994).
53. E. D. Swanner, A. M. Mloszewska, O. A. Cirpka, R. Schoenberg, K. O. Konhauser, A. Kappler, Modulation of oxygen production in Archaean oceans by episodes of Fe(II) toxicity. *Nat. Geosci.* **8**, 126–130 (2015).
54. A. M. Mloszewska, D. B. Cole, N. J. Planavsky, A. Kappler, D. S. Whitford, G. W. Owttrim, K. O. Konhauser, UV radiation limited the expansion of cyanobacteria in early marine photic environments. *Nat. Commun.* **9**, 3088 (2018).
55. G. J. Dick, S. L. Grim, J. M. Klatt, Controls on O₂ production in cyanobacterial mats and implications for Earth's oxygenation. *Annu. Rev. Earth Planet. Sci.* **46**, 123–147 (2018).
56. A. H. Knoll, R. K. Bambach, Directionality in the history of life: Diffusion from the left wall or repeated scaling of the right? *Paleobiology* **26**, 1–14 (2000).
57. J. Zhang, P. D. Quay, D. O. Wilbur, Carbon isotope fractionation during gas-water exchange and dissolution of CO₂. *Geochim. Cosmochim. Acta* **59**, 107–114 (1995).
58. C. S. Romanek, E. L. Grossman, J. W. Morse, Carbon isotopic fractionation in synthetic aragonite and calcite: Effects of temperature and precipitation rate. *Geochim. Cosmochim. Acta* **56**, 419–430 (1992).
59. T. M. Lenton, S. J. Daines, B. J. W. Mills, COPSE reloaded: An improved model of biogeochemical cycling over Phanerozoic time. *Earth Sci. Rev.* **178**, 1–28 (2018).
60. A. P. Gumsley, K. R. Chamberlain, W. Bleeker, U. Söderlund, M. O. de Kock, E. R. Larsson, A. Bekker, Timing and tempo of the Great Oxidation Event. *Proc. Natl. Acad. Sci.* **114**, 1811–1816 (2017).
61. C. J. Bjerrum, D. E. Canfield, Ocean productivity before about 1.9 Gyr ago limited by phosphorus adsorption onto iron oxides. *Nature* **417**, 159–162 (2002).
62. K. Fennel, M. Follows, P. G. Falkowski, The co-evolution of the nitrogen, carbon and oxygen cycles in the Proterozoic ocean. *Am. J. Sci.* **305**, 526–545 (2005).
63. A. D. Anbar, A. H. Knoll, Proterozoic ocean chemistry and evolution: A Bioinorganic bridge? *Science* **297**, 1137–1142 (2002).

64. D. T. Johnston, F. Wolfe-Simon, A. Pearson, A. H. Knoll, Anoxygenic photosynthesis modulated Proterozoic oxygen and sustained Earth's middle age. *Proc. Natl. Acad. Sci.* **106**, 16925–16929 (2009).

65. N. J. Butterfield, Oxygen, animals and oceanic ventilation: An alternative view. *Geobiology* **7**, 1–7 (2009).

66. P. Sánchez-Baracaldo, A. Ridgwell, J. A. Raven, A Neoproterozoic transition in the marine nitrogen cycle. *Curr. Biol.* **24**, 652–657 (2014).

67. T. L. Hamilton, D. A. Bryant, J. L. Macalady, The role of biology in planetary evolution: Cyanobacterial primary production in low-oxygen Proterozoic oceans. *Environ. Microbiol.* **18**, 325–340 (2016).

68. J. F. Allen, B. Thake, W. F. Martin, Nitrogenase inhibition limited oxygenation of Earth's proterozoic atmosphere. *Trends Plant Sci.* **24**, 1022–1031 (2019).

69. R. E. Summons, J. M. Hayes, Principles of molecular and isotopic biogeochemistry, in *The Proterozoic Biosphere, a Multidisciplinary Study*, J. W. Schopf, C. Klein, Eds. (Cambridge Univ. Press, 1992), pp. 83–94.

70. S. E. Stevens Jr., C. O. P. Patterson, J. Myers, The production of hydrogen peroxide by blue-green algae: A survey¹. *J. Phycol.* **9**, 427–430 (1973).

71. R. E. Zeebe, D. Wolf-Gladrow, *CO₂ in Seawater: Equilibrium, Kinetics, Isotopes* (Oceanography Series, Elsevier, ed. 1, 2001), vol. 65.

72. C. G. Trick, S. W. Wilhelm, Physiological changes in the coastal marine cyanobacterium *Synechococcus* sp. PCC 7002 exposed to low ferric ion levels. *Mar. Chem.* **50**, 207–217 (1995).

73. R. D. Guy, M. L. Fogel, J. A. Berry, Photosynthetic fractionation of the stable isotopes of oxygen and carbon. *Plant Physiol.* **101**, 37–47 (1993).

74. D. B. McNevin, M. R. Badger, S. M. Whitney, S. von Caemmerer, G. G. B. Tcherkez, G. D. Farquhar, Differences in carbon isotope discrimination of three variants of D-ribulose-1,5-bisphosphate carboxylase/oxygenase reflect differences in their catalytic mechanisms. *J. Biol. Chem.* **282**, 36068–36076 (2007).

75. R. L. Clark, J. C. Cameron, T. W. Root, B. F. Pfleger, Insights into the industrial growth of cyanobacteria from a model of the carbon-concentrating mechanism. *AIChE J.* **60**, 1269–1277 (2014).

76. P. J. Thomas, A. J. Boller, S. Satagopan, F. R. Tabita, C. M. Cavanaugh, K. M. Scott, Isotope discrimination by form IC RubisCO from *Ralstonia eutropha* and *Rhodobacter sphaeroides*,

metabolically versatile members of '*Proteobacteria*' from aquatic and soil habitats. *Environ. Microbiol.* **21**, 72–80 (2019).

77. E. B. Wilkes, A. Pearson, A general model for carbon isotopes in red-lineage phytoplankton: Interplay between unidirectional processes and fractionation by RubisCO. *Geochim. Cosmochim. Acta* **265**, 163–181 (2019).

78. R. E. Zeebe, On the molecular diffusion coefficients of dissolved CO_2 , HCO_3^- , and CO_3^{2-} and their dependence on isotopic mass. *Geochim. Cosmochim. Acta* **75**, 2483–2498 (2011).

79. M. H. O'Leary, Measurement of the isotope fractionation associated with diffusion of carbon dioxide in aqueous solution. *J. Phys. Chem.* **88**, 823–825 (1984).